# Reactive Autophobic Spreading of Drops

John K. Hunter
Department of Mathematics and
Institute of Theoretical Dynamics
University of California at Davis
Davis, CA 95616
jkhunter@ucdavis.edu

Zhilin Li
Center for Research in Scientific Computation
and Department of Mathematics
North Carolina State University
Raleigh, NC 27695
zhilin@math.ncsu.edu

Hongkai Zhao
Department of Mathematics
University of California
Irvine, 92697
zhao@math.uci.edu

**Abstract**

We use a lubrication theory approximation to formulate a model for the reactive spreading of drops that deposit an autophobic monolayer of surfactant on a surface. The model consists of a Poisson equation on a moving domain with boundary conditions that depend on the history of the domain motion. We develop a numerical algorithm for solving the model, using the immersed interface method and the level set method. Numerical solutions for traveling drops are qualitatively similar to experimental observations of reactive autophobic spreading.

## 1 Introduction

When a liquid drop of a solution of the surfactant hexadecanethiol (HDT) in hexadecane is placed on a gold surface, the drop deposits an HDT monolayer on the gold, which affects the wetting properties of the surface. For a wide range of HDT concentrations, the drop moves spontaneously over the surface, a phenomenon called reactive autophobic spreading [2]. The motion of the drop is caused by the difference between the static contact angles at the front of the drop, where the liquid spreads out over the gold surface, and the rear of the drop, where the liquid retracts on the HDT monolayer deposited during its passage. The deposition of self-assembled monolayers of organic films by drops has significant potential for the preparation of surfaces in a variety of industrial applications [2, 4, 5].

In this paper, we formulate a model, based on Greenspan's lubrication theory approximation [12], that describes the coupling between the motion of a drop and the deposition of a surfactant monolayer. The model consists of a Poisson equation for the drop height on a moving domain, together with conditions for the velocity of the domain boundary that incorporate the effect of surfactant deposition. We develop a numerical scheme to compute solutions of the model, using an immersed interface method to solve the Poisson equation, and a level set method to evolve the moving domain. The numerical solutions include traveling drops that are qualitatively similar to those observed in experiments.

The methods used here can be adapted to treat other problems in which a liquid drop affects the wetting properties of the surface on which it moves. For example, a solvent drop on a polymer surface may solvate or swell the surface [1], and in metallurgy a solder drop on a metal substrate or a molten metal drop on a ceramic substrate may react with the substrate (see [3, 9], for example). More generally, the level set approach should be useful in a wide variety of problems involving drop motion, which are often analyzed in a one-dimensional approximation because of the analytical difficulties in treating the geometry of a two-dimensional wetted region. Similar methods may also be useful in the study of cell motion in biology. For example, some of our numerical solutions for the evolution of drops resemble the motile behavior of keratocyte cells in wound healing [16]. These cells deposit an actin network on the surface over which they move [23], in an analogous way to the deposition of surfactant by a drop.

## 2 The model

To model the motion of the drop, we make the following assumptions.

1. The drop has constant mean curvature $\kappa(t)$ at each time $t$.
2. The drop volume $Q$ is constant in time.
3. The drop is thin and the dynamic contact angle $\theta$ is small.

The first assumption can be derived from the incompressible Navier-Stokes equations under certain approximations, including lubrication theory, and sufficiently slow motion of the drop [12]. The second assumption follows from the incompressibility of the fluid. The third assumption is consistent with the lubrication theory approximation. We consider a drop that moves on a horizontal surface, so we neglect the effect of gravity.

We denote the region of the surface wetted by the drop at time $t$ by $\Omega(t) \subset \mathbb{R}^2$. The contact line is the boundary $\partial\Omega(t)$ of $\Omega(t)$. We let $h(\vec{x}, t) > 0$ denote the height of the drop at a point $\vec{x} \in \Omega(t)$ at time $t$. Since the drop is thin, we may approximate the mean curvature of the drop surface by $-\Delta h$. The above assumptions imply that the wetted region $\Omega(t)$ and the drop height $h(\vec{x}, t)$ satisfy the following equations:

$$\begin{aligned} -\Delta h &= \kappa(t), && \vec{x} \in \Omega(t), \\ h &= 0, && \vec{x} \in \partial\Omega(t), \\ \textstyle\int_{\Omega(t)} h(\vec{x}, t)\, dA &= Q. \end{aligned} \tag{2.1}$$

Since the drop is thin, we approximate the macroscopic dynamic contact angle $\theta$ of the drop by

$$\tan\theta = |\nabla h|, \quad \text{or} \quad \theta = |\nabla h|. \tag{2.2}$$

The second relation above is valid if $|\nabla h|$ is small and will be used in the perturbation analysis in the next section. For numerical simulations, we can use either of the relations.

We assume that the outward normal velocity $V_n$ of the contact line depends on the dynamic contact angle. A convenient choice for this dependence is [6]

$$V_n = \begin{cases} K\,(\theta - \theta_A)^m & \text{if } \theta \geq \theta_A, \\ 0 & \text{if } \theta_R < \theta < \theta_A, \\ -K\,(\theta_R - \theta)^m & \text{if } \theta \leq \theta_R. \end{cases} \tag{2.3}$$

Here, $\theta_A \geq \theta_R$ denote the advancing and receding contact angles, respectively, and $K > 0$, $m \geq 1$ are constants.

To model the effect of surfactant deposition, we suppose that the advancing and receding contact angles are a function of the time $\tau(\vec{x}, t)$ that a point $\vec{x}$ has been wetted by the drop up to time $t$. For definiteness, we suppose that

$$\theta_A(\vec{x}, t) = \theta_{AM} F\left(\frac{\tau(\vec{x}, t)}{T_M}\right), \qquad \theta_R(\vec{x}, t) = \theta_{RM} F\left(\frac{\tau(\vec{x}, t)}{T_M}\right), \tag{2.4}$$

where the constants $\theta_{AM}$ and $\theta_{RM}$ are the advancing and receding contact angles, respectively, of the drop on a fully deposited monolayer, $T_M$ is a timescale for the deposition of the monolayer, and $F$ is a monotone increasing function with $F(0) = 0$, if the bare surface is perfectly wetting, and $F(+\infty) = 1$. The timescale $T_M$ depends on the concentration of the surfactant in the drop, with larger concentrations corresponding to smaller deposition timescales $T_M$. The deposition of a monolayer has a negligible effect on the concentration of surfactant, except possibly at low concentrations and large times, so we assume that $T_M$ is a constant. For our sharp interface formulation, the contact angle is only defined at the boundary of the wetted region $\Omega(t)$ and it is the difference between the dynamic contact angle and the advancing and receding contact angles respectively that drives the motion of the droplet. Of course there can be more complicated physics involved, such as flow inside the drop, boundary layers and precursor in front of the wetting boundary, that can affect the deposition of surfactants and the motion of the contact line. However we neglect them in our present model.

To write an expression for the wetting time $\tau$, we introduce the characteristic function $\chi_{\Omega(t)}$ of the wetted region, defined by

$$\chi_{\Omega(t)}(\vec{x}) = \begin{cases} 1, & \text{if } \vec{x} \in \Omega(t), \\ 0, & \text{if } \vec{x} \notin \Omega(t). \end{cases} \tag{2.5}$$

The wetting time function $\tau$ is given by

$$\tau(\vec{x}, t) = \tau_0(\vec{x}) + \int_0^t \chi_{\Omega(s)}(\vec{x})\, ds, \tag{2.6}$$

where $\tau_0(\vec{x})$ is the wetting time of $\vec{x}$ at $t = 0$.

Equations (2.1)–(2.6) are the model. The main new feature, in comparison with Greenspan's equations [12], is the dependence of the advancing and receding contact angles on the wetting time. We suppose that $Q$, $K$, $\theta_{AM}$, $\theta_{RM}$, $T_M$ are given parameters, and $F$ is a given function. The initial data are the wetted region $\Omega(0)$, and the wetting time $\tau_0(\vec{x})$. We want to find the wetted region $\Omega(t)$ at later times, together with the drop height $h(\vec{x}, t)$, the drop curvature $\kappa(t)$, and the wetting time $\tau(\vec{x}, t)$. The amount of surfactant deposited on the surface is determined by the wetting time.

While (2.1)–(2.6) is a simplified model for the problem, it does contain the essential components for the problem within certain realistic parameter range. This is backed up by the agreement between the experimental data (Figure 17) and our simulations ( Figure 16 and Figure 18).

To identify the dimensionless parameters in the problem, we let $L$ be a characteristic diameter of the wetted region $\Omega(t)$, and $H$ a characteristic height of the drop. A characteristic angle is then $\Theta = H/L$, and a characteristic velocity scale associated with the "pulling" of the contact line is

$$U = K\Theta^m.$$

As a characteristic timescale for the drop motion, we use

$$T_D = \frac{L}{U}.$$

Denoting dimensionless variables by a bar, we define

$$\bar{\vec{x}} = \frac{\vec{x}}{L}, \quad \bar{t} = \frac{t}{T_D}, \quad \bar{h} = \frac{h}{H}, \quad \bar{\kappa} = \frac{L^2\kappa}{H}, \quad \bar{\theta} = \frac{\theta}{\Theta}, \quad \bar{\theta}_A = \frac{\theta_A}{\Theta}, \quad \bar{\theta}_R = \frac{\theta_R}{\Theta}, \quad \bar{\tau} = \frac{\tau}{T_D}.$$

Transforming (2.1)–(2.6) into the barred variables, then dropping all bars, we find that the dimensionless problem is

$$\begin{aligned} -\Delta h &= \kappa(t), && \vec{x} \in \Omega(t), \\ h &= 0, && \vec{x} \in \partial\Omega(t), \\ \textstyle\int_{\Omega(t)} h(\vec{x},t)\, dA &= q, \end{aligned} \tag{2.7}$$

where the order one parameter $q$ is given by

$$q = \frac{Q}{HL^2}. \tag{2.8}$$

The contact line velocity is given by

$$V_n = \begin{cases} (|\nabla h| - \theta_A)^m & \text{if } |\nabla h| \geq \theta_A, \\ 0 & \text{if } \theta_R < |\nabla h| < \theta_A, \\ -(\theta_R - |\nabla h|)^m & \text{if } |\nabla h| \leq \theta_R, \end{cases} \qquad \vec{x} \in \partial\Omega(t), \tag{2.9}$$

$$\theta_A = f_A(\tau), \qquad \theta_R = f_R(\tau), \tag{2.10}$$

where $\tau$ is given by (2.6), and the advancing and receding contact angle functions $f_A$, $f_R$ are given by

$$f_A(\tau) = \alpha_A F\left(\frac{\tau}{T}\right), \qquad f_R(\tau) = \alpha_R F\left(\frac{\tau}{T}\right).$$

Here, the dimensionless parameters $\alpha_A$, $\alpha_R$, $T$ are defined by

$$\alpha_A = \frac{\theta_{AM}}{\Theta}, \qquad \alpha_R = \frac{\theta_{RM}}{\Theta}, \qquad T = \frac{T_M}{T_D}.$$

The most important parameter is $T$, which is the ratio of a timescale $T_M$ for the monolayer deposition and a timescale $T_D$ for the motion of the drop. Higher surfactant concentrations correspond to more rapid deposition, and therefore to smaller values of $T$.

In most of our solutions, we will neglect contact-angle hysteresis (for reasons stated below), meaning that $\theta_A = \theta_R$, and assume a linear relation between the contact line velocity and dynamic contact angle, corresponding to $m = 1$ in (2.9). In that case, we may write

$$V_n = |\nabla h| - \theta_S, \tag{2.11}$$

$$\theta_S = f(\tau), \tag{2.12}$$

where

$$f(\tau) = \alpha F\left(\frac{\tau}{T}\right)$$

and $\alpha$, $T$ are parameters.

A simple choice of the functions $F$ and $f$, which describe a surface that is perfectly wetting in the absence of a monolayer, is given by

$$F(t) = \begin{cases} t, & \text{if } 0 \le t \le 1, \\ 1, & \text{if } t > 1, \end{cases} \qquad f(\tau) = \begin{cases} \alpha\tau/T, & \text{if } 0 \le \tau \le T, \\ \alpha, & \text{if } \tau > T. \end{cases} \tag{2.13}$$

It is useful to reformulate the problem, both for the analysis and for the numerical computations, by introducing a scaled height function $\psi$, defined by

$$\psi(\vec{x}, t) = \frac{h(\vec{x}, t)}{\kappa(t)}. \tag{2.14}$$

Elimination of $h$ from (2.7) gives the following problem for $\psi$:

$$\begin{aligned} -\Delta\psi &= 1, \qquad && \vec{x} \in \Omega(t), \\ \psi &= 0, && \vec{x} \in \partial\Omega(t). \end{aligned} \tag{2.15}$$

Considering the case (2.11), for simplicity, the contact line velocity is determined from

$$\begin{aligned} V_n &= \kappa|\nabla\psi| - \theta_S \qquad \vec{x} \in \partial\Omega(t), \\ \kappa(t) &= \frac{q}{\int_{\Omega(t)} \psi(\vec{x}, t)\, d\vec{x}}, \end{aligned} \tag{2.16}$$

where the static contact angle $\theta_S$ is given by (2.6) and (2.12). The height function $h$ may be recovered from $\psi$ and $\Omega$ by

$$h(\vec{x}, t) = \frac{q\psi(\vec{x}, t)}{\int_{\Omega(t)} \psi(\vec{y}, t)\, d\vec{y}}. \tag{2.17}$$

Finally, we consider in more detail the applicability of the above assumptions to the experiments on reactive autophobic spreading reported in [2]. Hexadecanethiol (HDT) and hexadecane are organic liquids with similar surface tension and viscosity. Hexadecane is perfectly wetting on a gold surface, and a pure hexadecane drop spreads out into a thin uniform film, which eventually breaks up. HDT deposits a self-assembled monolayer (SAM) on a gold surface, and both HDT and hexadecane are partially wetting on the SAM. When a drop of pure HDT is placed on a gold surface, it deposits a SAM, then retracts on the SAM into a stationary drop. This phenomenon is called autophobic pinning. A drop that consists of a solution of HDT in hexadecane, with a concentration between about 1 $\mu$M and 0.1 M, travels across the surface with a roughly constant shape and velocity until the entire surface is covered by a SAM, or until the HDT in the drop is depleted.

The drop shown in Fig. 17 from [2] consists of a 1 mM solution of HDT in hexadecane, with a diameter of approximately 1 mm. After about 1 s of contact with the gold surface, the drop starts to move, then accelerates until it travels with a constant velocity $U$ of the order 1 mm/s. The viscosity $\mu$ and the surface tension $\sigma$ of hexadecane, at 25 C, are approximately $\mu = 3$ mPa s and $\sigma = 30$ mN/m [22]. The small value of the corresponding capillary number, $C = U\mu/\sigma = 10^{-4}$, indicates that surface tension forces dominate viscous forces in the motion of a drop, except in the immediate vicinity of the contact line [24]. Surfactants on the surface of the drop may play a role

in the experiments, for example by inducing Marangoni effects, but since surfactant deposition on the solid surface is the primary cause of the drop motion, it is reasonable to begin with a quasi-static model and assume that the mean curvature of the drop depends only on time.

The measured contact angle at the front of the traveling drop in Fig. 5 of [2] is less than 5°, while at the rear it is approximately 40°. The rear angle is too large to expect that lubrication theory applies quantitatively, but in view of the resulting simplifications, it is a valuable qualitative model. For smaller HDT concentrations, the monolayer at the rear of the drop is not fully organized, and the receding contact angle is less, so a lubrication theory approximation should be more accurate.

The deformation and motion of the drop is caused by the large difference between the static contact angles of the unwetted gold surface onto which the drop spreads and the SAM at the rear of the drop from which it retracts. This difference is much larger than the difference between the advancing and receding contact angles of the drop on a fully deposited SAM. The advancing contact angle of HDT on a fully deposited HDT monolayer is approximately 53°, and the receding contact angle is approximately 46°. These considerations suggest that it is reasonable to neglect contact angle hysteresis in a first approximation.

We could use other relations for the dependence of the contact line velocity on the dynamic contact angle, as well as more detailed models for the fluid flow near the contact line [8, 13, 14, 24, 27]. Our main interest, however, is in studying the global effect of surfactant deposition on the bulk motion and deformation of the drop, and we will not investigate other contact line models here.

# 3 Analytical solutions

In this section, we give some analytical solutions of the model equations that illustrate the reactive spreading of drops, or that are useful in testing the numerical scheme.

## 3.1 Circular drops

Equations (2.15)–(2.16) have an exact equilibrium solution for a drop with a circular wetted region on a surface with constant static contact angle $\theta_S = \theta_0 > 0$. We use polar coordinates $(r, \vartheta)$. The equilibrium radius of the wetted region is $r = a_0$ where

$$a_0 = \left(\frac{4q}{\pi\theta_0}\right)^{1/3}. \tag{3.1}$$

The scaled height function of the drop is $\psi = \psi_0(r)$, and the mean curvature is $\kappa = \kappa_0$, where

$$\psi_0(r) = \frac{1}{4}\left(a_0^2 - r^2\right), \qquad \kappa_0 = \frac{8q}{\pi a_0^4}. \tag{3.2}$$

Two exact solutions for circular wetted regions and the linear stability analysis of the above equilibrium solutions are given in [12]. The exact solutions are useful for testing our numerical method. In the first solution, we suppose that the static contact angle $\theta_0$ is constant, and the initial shape of the wetted region is a circle whose radius $r_0$ is different from equilibrium radius

$a_0$ in (3.1). The solution is a circular wetted region of radius $a(t)$, with

$$\psi = \frac{1}{4}\left(a^2 - r^2\right), \qquad \kappa = \frac{8q}{\pi a^4}, \qquad h = \frac{2q}{\pi a^4}\left(a^2 - r^2\right). \tag{3.3}$$

The radius $a(t)$ of the wetted region satisfies the ordinary differential equation,

$$\dot{a} = \theta_0 \left[\left(\frac{a_0}{a}\right)^3 - 1\right], \qquad a(0) = r_0. \tag{3.4}$$

If $r_0 < a_0$, the wetted region expands, while if $r_0 > a_0$ the wetted region contracts, and $a(t) \to a_0$ as $t \to +\infty$.

The second exact solution describes a circular wetted region moving across a surface whose static contact angle depends linearly on a Cartesian coordinate $x$. That is,

$$\theta_S = \theta_0 \left(1 - \lambda x\right), \tag{3.5}$$

where $\theta_0$ and $\lambda$ are constants. We assume that $\theta_S > 0$ in the wetted region. A solution of (2.7) is then given by a circular wetted region of radius $a(t)$, whose center is located at $(x, y) = (s(t), 0)$, where

$$\dot{a} = \theta_0 \left[\left(\frac{a_0}{a}\right)^3 - 1 + \lambda s\right], \qquad \dot{s} = \lambda \theta_0 a. \tag{3.6}$$

Here, $a_0$ is defined in (3.1). For small $\lambda$, the radius approaches a value close to $a_0$ and the circle then moves slowly to the right with velocity $\dot{s} \sim \lambda \theta_0 a_0$.

### 3.2 Traveling drops

In this subsection, we formulate a free boundary value problem for the shape of the wetted region of a drop that travels with constant velocity without change of shape. We use the perturbation method of Greenspan [12] to solve this problem in the case of a nearly circular wetted region on a partially wetting surface.

We denote the wetted region in a reference frame moving with the drop by $\Omega$. We use Cartesian coordinates $\vec{x} = (x, y)$ or $\vec{\xi} = (\xi, \eta)$ on the surface, and suppose that the drop velocity is $\vec{V} = V\vec{e}_x$, where $V > 0$ and $\vec{e}_x$ is the unit vector in the $x$-direction.

Given a point $\vec{x} \in \Omega$, we define $\lambda_\Omega(\vec{x})$ to be the length of the horizontal segment to the right of $\vec{x}$ which intersects $\Omega$. That is,

$$\lambda_\Omega(\vec{x}) = \mathcal{L}^1\left(I_\Omega[\vec{x}]\right), \tag{3.7}$$

where $\mathcal{L}^1$ denotes one-dimensional Lebesgue measure, and $I_\Omega[\vec{x}]$ is the set defined by

$$I_\Omega\left[(x, y)\right] = \left\{(\xi, \eta) \in \Omega : \xi > x \text{ and } \eta = y\right\}.$$

The wetting time $\tau(\vec{x})$ at a point $\vec{x}$ in the reference frame moving with the drop is given by

$$\tau(\vec{x}) = \frac{\lambda_\Omega(\vec{x})}{V}.$$

From (2.12), the static contact angle at $\vec{x} \in \partial\Omega$, i.e., the contact line, is

$$\theta_S(\vec{x}) = f\left(\frac{\lambda_\Omega(\vec{x})}{V}\right). \tag{3.8}$$

The unit outward normal $\vec{n}$ to the boundary of the wetted region is given in terms of the scaled height function $\psi$ by

$$\vec{n} = -\frac{\nabla\psi}{|\nabla\psi|}. \tag{3.9}$$

It follows that the normal velocity of the contact line is given by

$$V_n = -V\frac{\psi_x}{|\nabla\psi|}. \tag{3.10}$$

Using (3.8) and (3.10) in (2.11) and (2.15), we obtain the free boundary value problem,

$$\begin{aligned} -\Delta\psi &= 1, && \vec{x} \in \Omega, \\ \psi &= 0, && \vec{x} \in \partial\Omega, \\ \kappa_0|\nabla\psi| + V\frac{\psi_x}{|\nabla\psi|} &= f\left(\frac{\lambda_\Omega(\vec{x})}{V}\right), && \vec{x} \in \partial\Omega, \end{aligned} \tag{3.11}$$

where $\kappa_0$ is the constant mean curvature of the traveling drop, and $\lambda_\Omega$ is defined in (3.7). The problem is to find a speed $V$, a region $\Omega \subset \mathbb{R}^2$, and a scaled height function $\psi$ that satisfy (3.11), where $\kappa_0$ is a given constant and $f$ is a given nonnegative, monotonic increasing function.

When the bare surface is partially wetting and the effect of the surfactant is weak, we can solve this free boundary value problem by perturbing off the circular, equilibrium solution in (3.1)–(3.2). We suppose that the contact angle function $f$ in (3.11) is given by

$$f(\tau) = \theta_0 + \epsilon g(\epsilon\tau), \tag{3.12}$$

where $\theta_0 > 0$ is a positive constant, $\epsilon$ is a small parameter, and $g(t)$ is an increasing function of $t$ with $g(0) = 0$. We use polar coordinates $(r, \vartheta)$. When $\epsilon = 0$, an exact solution of (3.11) is given by $\Omega = \Omega_0$, $\psi = \psi_0(r)$, and $V = 0$, where

$$\Omega_0 = \{(r,\vartheta) : r < a_0\}, \qquad \psi_0(r) = \frac{1}{4}\left(a_0^2 - r^2\right), \qquad a_0 = \frac{2\theta_0}{\kappa_0}. \tag{3.13}$$

For small $\epsilon$, we write the equation of the perturbed contact line $\partial\Omega$ as

$$r = a_0 + \epsilon b(\vartheta) + O(\epsilon^2), \tag{3.14}$$

and look for an asymptotic solution of (3.11) of the form

$$\begin{aligned} &\psi = \psi_0(r) + \epsilon\psi_1(r,\vartheta) + O(\epsilon^2), \\ &V = \epsilon V_1 + O(\epsilon^2), \\ &\lambda_\Omega = \lambda_0 + O(\epsilon). \end{aligned} \tag{3.15}$$

Here, $\lambda_0$ is the length function (3.7) of the circular domain $\Omega_0$, which is given by

$$\lambda_0(\vartheta) = \begin{cases} -2a_0\cos\vartheta, & \text{if } \pi/2 \le \vartheta \le 3\pi/2, \\ 0, & \text{if } -\pi/2 \le \vartheta \le \pi/2. \end{cases} \tag{3.16}$$

We use (3.12)–(3.15) in (3.11), Taylor expand the result with respect to $\epsilon$, and equate coefficients of $\epsilon$. After some algebra, we find that

$$\begin{aligned} -\Delta\psi_1 &= 0, && \text{in } r < a_0, \\ \psi_1 &= \frac{1}{2}a_0 b, && \text{on } r = a_0, \\ \kappa_0\psi_{1r} &= \frac{1}{2}\kappa_0 b - V_1\cos\vartheta - g\left(\frac{\lambda_0}{V_1}\right), && \text{on } r = a_0. \end{aligned} \tag{3.17}$$

The first two equations of (3.17) imply that $\psi_{1r}|_{r=a_0}$ is given in terms of $b$ by

$$\psi_{1r}|_{r=a_0} = \frac{1}{2}\mathcal{K}[b], \tag{3.18}$$

where the Dirichlet-to-Neumann operator $\mathcal{K}$ is defined by

$$\mathcal{K}\left[\sum_{n=-\infty}^{\infty} b_n e^{in\vartheta}\right] = \sum_{n=-\infty}^{\infty} |n| b_n e^{in\vartheta}. \tag{3.19}$$

The use of (3.18) in the third equation of (3.17) implies that $b$ satisfies

$$\frac{1}{2}\kappa_0\left\{b - \mathcal{K}\left[b\right]\right\} = G(\vartheta, V_1), \tag{3.20}$$

where

$$G(\vartheta, V_1) = V_1\cos\vartheta + g\left(\frac{\lambda_0(\vartheta)}{V_1}\right). \tag{3.21}$$

We expand $b$ and $G$ in Fourier series,

$$b = \sum_{n=-\infty}^{\infty} b_n e^{in\vartheta}, \qquad G = \sum_{n=-\infty}^{\infty} G_n e^{in\vartheta}. \tag{3.22}$$

From (3.16) and (3.21), we have $G_{-n} = G_n$ and

$$\begin{aligned} G_1 &= \frac{1}{2}V_1 - \frac{1}{\pi}\int_0^{\pi/2} g\left(\frac{2a_0}{V_1}\cos\vartheta\right)\cos\vartheta\, d\vartheta, \\ G_n &= \frac{(-1)^n}{\pi}\int_0^{\pi/2} g\left(\frac{2a_0}{V_1}\cos\vartheta\right)\cos n\vartheta\, d\vartheta, \qquad \text{if } |n| \neq 1. \end{aligned} \tag{3.23}$$

The use of equations (3.19) and (3.22) in (3.20) implies that

$$\frac{1}{2}\kappa_0\left(1 - |n|\right)b_n = G_n. \tag{3.24}$$

Thus, equation (3.20) is solvable for $b$ if and only if $G_1 = 0$. From (3.23), it follows that the first order drop velocity $V_1$ satisfies the equation

$$V_1 = \frac{2}{\pi}\int_0^{\pi/2} g\left(\frac{2a_0}{V_1}\cos\vartheta\right)\cos\vartheta\, d\vartheta. \tag{3.25}$$

Since the right-hand side of (3.25) is a positive decreasing function of $V_1$, this equation has a unique positive solution for $V_1$.

The solution of (3.20) is not unique, since $b_1$ is arbitrary. This Fourier coefficient corresponds to a small translation of the drop, and we set it equal to zero for simplicity. From (3.22) and (3.24), the location of the contact line is then given by (3.14) with

$$b(\vartheta) = \frac{2G_0}{\kappa_0} - \frac{4}{\kappa_0} \sum_{n=2}^{\infty} \frac{G_n}{n-1} \cos n\vartheta.$$

For example, suppose that the contact angle function $f$ is a linear function of the wetting time,

$$f(\tau) = \theta_0 + \epsilon^2 \tau. \tag{3.26}$$

This function is a Taylor approximation of more general contact angle functions in a slow deposition limit on a partially wetting surface. The corresponding function $g$ in (3.12) is

$$g(t) = t. \tag{3.27}$$

Using (3.27) in (3.25) and solving the resulting equation, we find that $V_1 = a_0^{1/2}$. Thus, from (3.15), the velocity of the traveling drop is

$$V = \epsilon a_0^{1/2} + O(\epsilon^2). \tag{3.28}$$

The square-root dependency of the drop velocity on the radius is a consequence of the following scalings: (a) the drop velocity is proportional to the difference between the static contact angles at the rear of the drop and the front of the drop; (b) the static contact angle difference is proportional to the passage time of the drop; (c) the drop passage time is proportional to the radius of the wetted region and inversely proportional to the drop velocity.

When $g$ is given by (3.27), the perturbation $b$ of the contact line is given by

$$b(\vartheta) = \frac{8a_0^{1/2}}{\pi\kappa_0} \left\{ \frac{1}{2} + \sum_{m=1}^{\infty} \frac{(-1)^m}{(2m-1)(4m^2-1)} \cos 2m\vartheta \right\}. \tag{3.29}$$

From (3.14) and (3.29), the $x$-diameter $d_x$ and the $y$-diameter $d_y$ of the wetted region are given by

$$d_x = 2a_0 + \frac{8\epsilon a_0^{1/2}}{\pi\kappa_0}(1+2D) + O(\epsilon^2), \qquad d_y = 2a_0 + \frac{8\epsilon a_0^{1/2}}{\pi\kappa_0}(1+2S) + O(\epsilon^2), \tag{3.30}$$

where

$$D = \sum_{m=1}^{\infty} \frac{(-1)^m}{(2m-1)(4m^2-1)}, \qquad S = \sum_{m=1}^{\infty} \frac{1}{(2m-1)(4m^2-1)}.$$

The numerical values of $D$ and $S$ are $D \approx -0.315$ and $S \approx 0.366$. Thus, the mean diameter of the wetted region is larger than the equilibrium diameter of the circular wetted region of a drop with the same mean curvature on a surface with uniform static contact angle $\theta_0$, and the drop is elongated in the direction orthogonal to its direction of motion. In Sec. 5.2, we compare this

asymptotic solution with a numerical solution for a nearly circular traveling drop (see Fig. 10 and Table 3).

We cannot obtain a solution for traveling drops on a perfectly wetting surface in this way, because there is no equilibrium solution in that case. In fact, there cannot be any traveling drop solutions with smooth contact lines on a perfectly wetting surface. To see this, suppose for contradiction that the wetted region $\Omega$ of the traveling drop belongs to the Hölder class $C^{2,\alpha}$ for some $\alpha > 0$. It then follows [11] that the solution of $-\Delta\psi = 1$ for the scaled height function satisfies $\psi \in C^{2,\alpha}(\overline{\Omega})$. If the drop travels in the $x$-direction, then at a top or bottom point of the contact line $\partial\Omega$ where $y$ has an extreme value, then the gradient of $\psi$ must equal zero, since otherwise the contact line would move outwards in the $y$-direction, contradicting the assumption that the wetted region moves without change of shape. We introduce local orthogonal coordinates $(s, n)$, where $s$ is arclength along the contact line and $n$ is a coordinate normal to the contact line. Then since $\Delta\psi < 0$ and $\psi = 0$ on $\partial\Omega$, we see that $\psi_{nn} < 0$ at the extreme point, which implies the contradiction that $\psi < 0$ inside the wetted region. This argument does not prove the nonexistence of traveling drops whose contact lines have cusps at the top and bottom edges, for example, but if such traveling drops exist, any smoothing of the cusps would destroy them.

# 4 The numerical method

In this section we combine the level set method and the immersed interface method to develop an Eulerian formulation to capture the shape and motion of reactive spreading drops on a fixed Cartesian grid. We extend the immersed interface method to solve the Possion equation on an arbitrary domain and modify the standard level set method to monitor the splitting or merging or droplets to enforce the volume conservation of each individual droplet instead of the total volume. The framework of our numerical algorithm can be easily adapted to models of more complicated physics and contact line dynamics.

We represent the moving contact line $\partial\Omega(t)$ as the zero level set of a two-dimensional level set function $\varphi(\vec{x}, t)$, such that

$$\Omega(t) = \{\, \vec{x} : \ \varphi(\vec{x}, t) < 0 \,\}, \qquad \partial\Omega(t) = \{\, \vec{x} : \ \varphi(\vec{x}, t) = 0 \,\}.$$

Given the level set function at some time, we solve the Poisson equation in (2.15) for the scaled height function $\psi$ by means of an immersed interface method, compute the normal velocity $V_n$ of the boundary from $\psi$, and update the level set function $\varphi$ by solving a Hamilton-Jacobi equation,

$$\varphi_t + V_n|\nabla\varphi| = 0. \tag{4.1}$$

An outline of one time step of the algorithm is as follows.

1. *Compute the drop height*

   - Use a modified fast immersed interface method, described in the next subsection, to solve the Poisson equation for $\psi$,

$$\begin{aligned} -\Delta\psi &= 1, \qquad \text{in } \Omega(t), \\ \psi &= 0, \qquad \text{on } \partial\Omega(t). \end{aligned}$$

- Compute the mean curvature $\kappa$ from volume conservation,

$$\kappa = \frac{q}{\int_{\Omega(t)} \psi \, dxdy},$$

  where $q$ is the drop volume. If there is more than one drop, then $\kappa$ is evaluated separately for each connected component of the set on which $\varphi$ is negative.

- The height of the drop is $h = \kappa \psi$.

2. *Compute the normal velocity at the boundary*

   - Use a weighted least squares interpolation algorithm to compute $\nabla h$ near the boundary, see [20].
   - Evaluate the static contact angle $\theta_S(\vec{x}, t)$ at the boundary.
   - Compute the normal velocity of the boundary, $V_n = |\nabla h| - \theta_S$.

3. *Evolve the contact line by use of a local level set method, and re-initialize if necessary.*

There is a subtlety in grid resolution for the wetting time when the static contact angle is affected by the surfactant deposition. Although the wetting time $\tau$ is continuous in space according to the definition (2.6), $|\nabla \tau| = \frac{1}{|V_n|}$. If the droplet is close to equilibrium solution or the contact line is moving slowly, we need fine grid resolution to resolve the wetting time and hence the static contact angle. In our numerical experiments, grid refinements are used to ensure the convergence. We now give a more detailed description of the immersed interface method and the level set method.

### 4.1 Fast Poisson solvers on irregular domains

In order to compute the drop height, we need to solve a Poisson equation on an irregular domain whose shape varies in time. We use a Poisson solver based on the the fast immersed interface method (IIM) developed in [20] and a modified version developed in [15]. The modification is needed because the original IIM in [18, 20] is designed for interface problems that are defined in the entire domain with discontinuities occur at the interface. The main idea of our method here is to extend a Poisson equation on an irregular domain $\Omega$ to a Poisson equation on a larger, rectangular domain $R \supset \Omega$. This procedure allows the use of fast Poisson solvers on a fixed Cartesian grid that does not depend on the shape of the irregular domain. The extension of the irregular domain $\Omega$, which may have several connected components $\Omega_i$, is illustrated in Fig. 1. In this sub-section, we will omit the time dependency for simplicity.

We extend the source term in the Poisson equation by zero outside $\Omega$, and impose zero Dirichlet conditions on the boundary $\partial R$ of the rectangle. We require that the normal derivative of the solution $\psi$ is continuous across the immersed boundary $\partial\Omega$ of the irregular domain, but we allow a finite jump $v$ in the solution itself. In the language of potential theory, this requirement is equivalent to the introduction of a double-layer source on $\partial\Omega$. This extension leads to the

following interface problem,

$$\begin{aligned} \Delta\psi &= \begin{cases} -1 & \text{if } \vec{x} \in \Omega, \\ 0 & \text{if } \vec{x} \notin \Omega, \end{cases} \\ [\psi_n] &= 0, \qquad \text{on } \partial\Omega, \\ [\psi] &= v, \qquad \text{on } \partial\Omega, \\ \psi &= 0, \qquad \text{on } \partial R, \end{aligned} \tag{4.2}$$

where $\psi_n$ denotes the normal derivative of $\psi$ on $\partial\Omega$, and $[\cdot]$ denotes the jump across $\partial\Omega$. We choose $v$ so that the solution $\psi$ of (4.2) satisfies the Dirichlet boundary condition

$$\psi^- = 0, \qquad \text{on } \partial\Omega, \tag{4.3}$$

where $\psi^-$ is the limiting value of $\psi$ on $\partial\Omega$ taken from the inside of $\Omega$.

To numerically compute the solution of (4.2)–(4.3) for $\psi$ and $v$, we discretize the immersed boundary $\partial\Omega$. This boundary is given as the zero level set of a level set function $\varphi(x, y)$. The level set function then is defined as a grid function $\varphi_{ij} = \varphi(x_i, y_j)$. Let

$$\begin{aligned} \varphi_{i,j}^{max} &= \max\{\varphi_{i-1,j}, \varphi_{i,j}, \varphi_{i+1,j}, \varphi_{i,j-1}, \varphi_{i,j+1}\}, \\ \varphi_{i,j}^{min} &= \min\{\varphi_{i-1,j}, \varphi_{i,j}, \varphi_{i+1,j}, \varphi_{i,j-1}, \varphi_{i,j+1}\}. \end{aligned} \tag{4.4}$$

We call $(x_i, y_j)$ as an ***irregular grid point*** if $\varphi_{i,j}^{max}\, \varphi_{i,j}^{min} \leq 0$. Otherwise the grid point is a regular grid point[1]. We then compute the projections $(x^*, y^*)$ of the irregular grid points onto the boundary, as illustrated in Fig. 2. The detailed algorithm for finding the projections is explained in [15, 21].

We denote the vector of the discretized values of $\psi$ on $R$ by $\Psi$, and the vector of the discretized values of the jump $v$ at the projections of the irregular grid points that lie inside the wetted region by $V$. On an $N \times N$ grid, the number of components $N_\Psi$ of $\Psi$ is approximately $N^2$, while the number of components $N_V$ of $V$ is of the order $N$. Using the IIM [18, 19] to discretize the interface problem (4.2), we get a system of $N_\Psi$ linear equations of the form

$$A\Psi + BV = F_1, \tag{4.5}$$

where $A$ is the discrete Laplacian matrix, using a five point stencil, $B$ is a sparse matrix, and the vector $F_1$ is a source term, whose components may differ from the values of $f$ at the irregular grid points. Discretizing the Dirichlet condition (4.3) on the immersed boundary $\partial\Omega$, we get a system of $N_V$ linear equations of the form

$$C\Psi + DV = F_2. \tag{4.6}$$

Thus, we obtain a system of equations for the solution $\Psi$ and the jump $V$ on the boundary,

$$\begin{bmatrix} A & B \\ C & D \end{bmatrix} \begin{bmatrix} \Psi \\ V \end{bmatrix} = \begin{bmatrix} F_1 \\ F_2 \end{bmatrix}. \tag{4.7}$$

[1] Whether a grid point is regular or irregular depends on the time level. In other words, the label is updated at different time step.

The Schur complement of (4.7) is

$$(D - CA^{-1}B)V = G, \tag{4.8}$$

where

$$G = F_2 - CA^{-1}F_1.$$

Equation (4.8) for $V$ is a much smaller system than equation (4.7) for $(\Psi, V)$. We solve (4.8) by the generalized minimum residual (GMRES) method. Each iteration of the GMRES method involves one matrix-vector multiplication by $A^{-1}$, which we compute by means of a call to a fast Poisson solver for (4.5) with a specified jump $V$ in the solution. Each iteration also involves one call to the interpolation scheme to evaluate the residual $R = C\Psi + DV - F_2$ of the boundary condition (4.6) for the iterate.

This Poisson solver for irregular domains is second order accurate. The number of calls to the fast Poisson solver on the rectangular domain is equal to the number of GMRES iterations, and is almost independent of the mesh size, although it may depend on the geometry of the domain.

The method described here applys to multi-connected domain if the boundary of the droplets is expressed in terms of a single level set function in which the domain is divided by two parts: the set of $\varphi(\mathbf{x}) > 0$, and the set of $\varphi(\mathbf{x}) < 0$.

We illustrate these statements with a numerical example. We solve the Poisson equation

$$\begin{aligned} -\Delta\psi &= 4, \qquad \text{in } \Omega, \\ \psi &= x^2 + y^2 + e^x \cos y, \qquad \text{on } \partial\Omega, \end{aligned} \tag{4.9}$$

on an elliptical domain

$$\Omega = \left\{(x, y) : x^2/a^2 + y^2/b^2 < 1\right\}. \tag{4.10}$$

The exact solution is

$$\psi(x, y) = x^2 + y^2 + e^x \cos y.$$

In Table 1, we show the maximum norm error $E(N)$ of the numerical solution on an $N \times N$ grid for various values of $N$. We also show the number of irregular grid points $n_1$, the number of irregular grid points inside the boundary of the ellipse $n_2$, which is equal to the dimension of (4.8), and the number of GMRES iterations $k$. The order of convergence is measured by

$$O = \frac{\log\left[E(N)/E(2N)\right]}{\log 2}. \tag{4.11}$$

This ratio in The results in Table 1 approaches number 2 as $N \to \infty$, which indicates second order convergence. The number of GMRES iterations decreases slightly as $N$ increases. The stopping criteria for GMRES iteration is $tol = 10^{-8}$.

### 4.2 A modified level set method

We use the level set method [25] to compute the motion of the wetted region associated with a drop. In the usual level set method, there is no need to keep explicit track of topological changes in the moving region. In our problem, however, if several drops are present, then they move

| $N$ | $E$ | $O$ | $n_1$ | $n_2$ | $k$ |
|---|---|---|---|---|---|
| 32 | $4.21465\ 10^{-3}$ | | 68 | 36 | 9 |
| 64 | $8.1371\ 10^{-4}$ | 2.3728 | 132 | 68 | 7 |
| 128 | $1.7614\ 10^{-4}$ | 2.2078 | 268 | 136 | 6 |
| 256 | $3.8196\ 10^{-5}$ | 2.2053 | 532 | 268 | 6 |
| 512 | $8.5548\ 10^{-6}$ | 2.1586 | 1068 | 538 | 5 |

Table 1: Results of a grid refinement study for the numerical solution of (4.9) on the domain (4.10) with $a = 0.5$ and $b = 0.15$. Here, $N$ is the number of grid lines in the $x$ and $y$ directions, $e$ is the maximum norm error of the numerical solution, $r$ is the ratio of successive errors, $n_1$ is the number of irregular grid points, $n_2$ is the number of irregular grid points inside the ellipse, and $k$ is the number of GMRES iterations.

independently of each other. We therefore need to modify the usual level set method so that we can detect the splitting and merging of drops. The identification of separate drops is not required when we solve the Poisson equation for $\psi$, but it is required when we use the volume constraint to calculate the mean curvature of the drops. The use of a single mean curvature for the whole collection of drops would allow the transfer of fluid volume between physically disconnected drops. Our modified level set method preserves the volume of each individual drop. When a new drop is formed from splitting of old drops, or two drops merge together, our algorithm adjusts the mean curvature automatically with the correct volume.

We use the following algorithm to identify the wetted regions associated with the drops. Suppose that the grid points are $(x_i, y_j)$ and the values of the level set function $\varphi(x_i, y_j)$ are positive in the unwetted region of the surface.

1. Choose any seed grid point $(x_i, y_j)$ with $\varphi(x_i, y_j) \leq 0$. Find all points among its four neighboring points $(x_{i\pm1}, y_{j\pm1})$ whose level set function value is nonpositive, and tag them. These points are in the same region as the seed point.

2. Use the newly tagged points as an expanding boundary. Tag their connected but untagged neighbors whose level set function values are nonpositive.

3. Continue this expansion process until no new neighboring points can be tagged. If all untagged grid points have positive values for the level set function, then there is only one drop, and we are done. Otherwise, choose any untagged grid point that has a nonpositive value for the level set function and repeat the process until no untagged point has nonpositive level set function values.

We also evaluate the integral $\int_{\Omega_p} \psi(\vec{x})\, d\vec{x}$ for each disconnected component $\Omega_p$ in the above identification process. Since each grid point needs to be visited once, the complexity of this algorithm is linear in the number of grid points. The array of the expanding boundary points which we use to tag new points is one dimension lower than that of the computational domain. To make the algorithm more efficient, we only track topological changes for the grid points $(x_i, y_j)$ near the contact line that satisfy $-\Delta x \leq \varphi(x_i, y_j) \leq 0$, where $\Delta x$ is the grid size. The CFL condition for the level set equation ensures that we do not miss any topological changes.

When we detect that a drop has split into two, we use the above algorithm to identify the wetted regions $\Omega_1$ and $\Omega_2$ of the two new drops. Solution of the Poisson equation gives the scaled height function $\psi$ on $\Omega = \Omega_1 \cup \Omega_2$. We then decompose the volume $q$ of the original drop into two separate volumes $q_1$ and $q_2$ such that $q_1 + q_2 = q$ in the following way,

$$q_1 = \frac{q \int_{\Omega_1} \psi(\vec{x})\, d\vec{x}}{\int_{\Omega} \psi(\vec{x})\, d\vec{x}}, \qquad q_2 = \frac{q \int_{\Omega_2} \psi(\vec{x})\, d\vec{x}}{\int_{\Omega} \psi(\vec{x})\, d\vec{x}}.$$

This splitting of the volume is based on the assumption that the mean curvature $\kappa$ and the height $h$ are continuous with time. Therefore the volume of the $i$th drop is proportional to $\int_{\Omega_i} \psi(\vec{x})\, d\vec{x}$. When two drops merge we simply identify them as one drop and set the volume of the new drop equal to the sum of the volumes of the old drops.

After these modifications, we use the local level set method and corresponding numerical algorithms in [21, 29], see also the narrow band level set method [26] and there references therein, to update the moving boundary, as follows.

1. Evaluate the normal velocity of the contact line from

$$V_n = \kappa |\nabla \psi| - \theta_S, \qquad \kappa(t) = \frac{q}{\int_{\Omega(t)} \psi(\vec{x}, t)\, d\vec{x}},$$

   at the projections of the irregular grid points for each individual drop.

2. Extend the velocity off the front to a neighboring computational tube that contains the contact line. In our implementation, we solve the following convection equation using an upwinding scheme to solve

$$\frac{\partial V_n}{\partial t} + \nabla V_n \cdot \frac{\nabla \varphi}{|\nabla \varphi|} sign(\varphi) = 0, \tag{4.12}$$

   see for example, [15, 29], where $sign(\varphi)$ denotes the sign of $\varphi$. Another approach that can be used is the fast marching method [26].

3. Re-initialize the level set function if necessary by solving

$$\frac{\partial \varphi}{\partial t} + (|\nabla \varphi| - 1) sign(\varphi) = 0, \tag{4.13}$$

   see [28, 29] for example. Note that there are other extension and reinitilization methods, particularly the fast marching method in the literature, see [26] and the references therein.

4. Adjust the time step according to the computed velocity.

# 5 Numerical experiments

In our numerical simulations, we embed the wetted region in a square, $-2 \le x,\ y \le 2$, or $-1.5 \le x,\ y \le 1.5$, or $0 \le x,\ y \le 1$. The spatial step size $\Delta x$ is the same in both the $x$ and $y$ directions. Most solutions are computed on a $100 \times 100$, $200 \times 200$, or $300 \times 300$ grid. The time step $\Delta t$ in the level set method is $\Delta t = \Delta x/(8.1)$. The tolerance for the GMRES iteration is $10^{-8}$. We use $\theta = |\nabla h|$ for most of simulations except for Fig. 12 and Fig. 18 in which $\theta = \tan^{-1}(|\nabla h|)$ is used. The difference in the results obtained from the two different formula is hardly noticeable. The computations were performed on an Ultra-1 Sun workstation.

### 5.1 Drop motion without surfactant

In this subsection we present examples of drops moving on surfaces whose static contact angle is constant in time. We assume that the contact line velocity

$$V_n = \theta - \theta_S \tag{5.1}$$

depends linearly on the dynamic contact angle $\theta$. In Fig. 3, we show two numerical solutions of drops with circular wetted regions approaching their equilibrium radius on a uniform surface with a static contact angle of $\theta_S = 0.2$. The drop volume is $q = 0.05\pi$, and the equilibrium radius (3.1) is $a_0 = 1$. The analytical solution is given in (3.3)–(3.4). In Fig. 3 (a), the initial radius is greater than one, and the drop contracts, while in Fig. 3 (b), the initial radius is less than one, and the drop expands.

We use this simple example to check the order of accuracy of our numerical algorithms. We carried out a grid refinement study for a fixed time ($t = 0.5$) and the final state ($t = 5$) of the expanding wetted region shown in Fig. 3 (b). We summarize the results in Table 2. where we show the maximum error $E(t)$ in the radius, defined as follows. Let $\mathcal{S}(\sqcup)$ be the set of irregular grid points and let $(x^*_{ij}(t), y^*_{ij}(t))$ denote the projection of $(x_i, y_j) \in \mathcal{S}$ on the boundary. Then

$$E(t) = \max_{\mathcal{S}(\sqcup)} \left\{ \left| \sqrt{(x^*_{ij})^2 + (y^*_{ij})^2} - a(t) \right| \right\}, \tag{5.2}$$

where $a(t)$ is the exact radius described in Section 3.1. As $t$ gets large, $a(t)$ approaches to $a_0$, the equilibrium radius. We use the numerical solution at $t = 0.5$, and at $t = 5$, which is very close to the steady state solution, to check the order. The order of convergence parameter $O$ is defined in (4.11). The results in Table 2 confirm that the computed position is accurate to order $(\Delta x)^2$. In Fig. 4, we show the history of the error between $0 \le t \le 0.5$. The magnitude of the error is $O(10^{-6})$ and does not change very much with time.

| $N$ | $E(t = 0.5)$ | $O$ |
|---|---|---|
| 40 | $1.3596\ 10^{-4}$ | |
| 80 | $2.3127\ 10^{-5}$ | 2.5555 |
| 160 | $4.6955\ 10^{-6}$ | 2.3002 |
| 320 | $1.1679\ 10^{-6}$ | 2.0074 |

| $N$ | $E(t = 5)$ | $O$ |
|---|---|---|
| 40 | $1.1039\ 10^{-3}$ | |
| 80 | $1.3798\ 10^{-4}$ | 3.000 |
| 160 | $3.5897\ 10^{-5}$ | 1.9426 |
| 320 | $9.3392\ 10^{-6}$ | 1.9425 |

Table 2: A grid refinement study for an expanding circle. Here, $N$ is the number of $x$ and $y$ grid lines, $E(t)$ is the maximum error in the radius at $t = 0.5$ and $t = 5$, defined in (5.2), and $O$ is the order of convergence parameter, defined in (4.11). The results confirm second order accuracy.

In Fig. 5, we show a numerical simulation of the motion of drops with circular wetted regions on a surface whose static contact angle $\theta_S$ is given by (3.5). The exact solution is given by (3.6). When $\lambda$ is small, as shown in Fig. 5(a), the drop moves slowly to the right, while the radius of the circular wetted region approaches to the value $a_0 = (0.2)^{1/3} = 0.585\cdots$ given by (3.1). If $\lambda$ is not small, the radius of the wetted region changes more rapidly, as shown in Fig. 5(b).

Since we use the level set method to capture the moving contact lines, we can "automatically" handle the merging or splitting of drops in our numerical computations. Note that topological changes and singularities are really challenging questions physically, mathematically and numerically, because most of the continuous models and numerical computations are not very faithful at

that instant. However, for a well-posed system, which is true for our problem from linear stability analysis, we can expect that the topological transition and its effect on the whole system is very localized both in time and space. It is beyond the scope of this paper to address these issues either physically or mathematically. We just try to show that using the level set method such topological changes can be handled in a simple way if the model is still true, and hopefully our method can provide a good continuation after topological changes. Also it may not be possible to resolve topological changes and singularities to arbitrary accuracy on any finite grid. However the resolution should be better and more fine features can be revealed when the grid becomes finer.

In Fig. 6, we start with a drop with an initial dumbbell like wetted region on a surface with uniform static contact angle $\theta_S = 0.2(radian)$. The surface plot of the solution to the normalized Poisson equation $-\Delta\psi = 1$ with $\psi = 0$ at the boundary is shown in Fig. 8. The real shape of the drop is scaled by its volume as in (2.17). Therefore, depending on the drop volume $q$ and the geometry of the contact line, the wetted region may expand, partially expand and partially contract, or contract. If the drop has a relatively large volume, $q = (0.05)\pi(0.5)^3$, the initial contact angle is larger than the static contact angle everywhere along the contact line, the wetted region expands, and kinks develop in the contact line, as shown in Fig. 6. Eventually, the wetted region becomes circular with an equilibrium radius $a_0 = 0.5$. If, however, the drop has a relatively small volume, $q = (0.05)\pi(0.2)^3$, the initial contact angle is smaller than the static contact angle at some places along the contact line, and the wetted region contracts at those places. In the solution shown in Fig. 7, the portion of the contact line near the thin neck (concave part) has a contact angle that is smaller than the static contact angle and retracts, and the initial drop splits into two small drops. As explained in Sec. 4.2, we take special care to redistribute the total volume to each new drop and to make sure each drop conserves its own volume. Due to the symmetry in our example, these two drops are equal and their wetted regions eventually converge to a disc of radius $a_0 = 0.2 * (0.5)^{1/3} = 0.16$. Fig. 8 is the surface plot of the solution to the normalized Poisson equation $-\Delta\psi = 1$ with $\psi = 0$ at the boundary of the initial dumbbell in Fig. 7.

Next we show the merging of two drops. We start with two drops whose wetted regions are ellipses,

$$\frac{(x-0.35)^2}{0.2^2} + \frac{(y-0.5)^2}{0.14^2} = 1, \qquad \frac{(x-0.65)^2}{0.12^2} + \frac{(y-0.5)^2}{0.24^2} = 1. \tag{5.3}$$

Again if the volumes of the two drops are large enough they will expand. Fig. 9 shows the evolution of the wetted region in such a case. When the two drops merge we have to sum their volumes and conserve the volume for the newly formed drop. While we have not attempted to model the physical processes involved in detail, our numerical scheme appears to capture a physically reasonable evolution process for the wetted region, in a quasi-static regime where the adjustment of the drop surface to one of constant mean curvature is much faster than other processes, even after the merging or splitting of drops.

## 5.2 Drop motion with surfactant

In this subsection, we present numerical solutions that include the effect of surfactant deposition. To explain our choice of initial data, we first discuss the initiation of traveling drops. In experiments (see Fig. 17 obtained from [2]), a circular drop placed on an unwetted gold surface expands

initially, then part of the advancing contact line pins and peels back, after which the contact line retracts on the SAM that the drop has deposited, thus setting the drop into motion. The direction in which the drop moves is arbitrary, and depends on where the contact line first pins. The macroscopic solution therefore depends very sensitively on small-scale effects that lead to pinning. Possible physical mechanisms for pinning include random thermal or mechanical vibrations, surface heterogeneities and roughness, and the deposition of a SAM ahead of the macroscopic contact line by vapor or a thin precursor film [10, 17]. An understanding of these phenomena requires a detailed study of the solid–liquid–vapor–surfactant system near the contact line, which we will not attempt in this paper.

According to the macroscopic model we use here, the wetted region of a drop placed on an initially unwetted, perfectly wetting surface always expands and spreads out over the surface. As a result, the motion of the contact line is never influenced by the effects of surfactant deposition. This exact solution is, however, sensitive to perturbations that cause part of the contact line to begin retracting. In our numerical solutions, we perturb the wetted region in a controlled way by introducing nonzero initial data for the wetting time on part of the surface, meaning that part of the surface is covered by surfactant. This initial data mimics a partially wetting surface heterogeneity that can set the drop into motion. Once the drop moves onto an initially unwetted part of the surface, the nonzero initial wetting time has no further direct influence on the drop, and the drop motion is sustained by the interaction of the drop with its own SAM.

First, we compare the asymptotic solution for a nearly circular traveling drop on a partially wetting surface, derived in Sec. 3.2, with a numerical solution. We use the static contact angle

$$\theta_S = \theta_0 + \epsilon^2 \tau, \tag{5.4}$$

where $\theta_0 = 0.2$ and $\epsilon = 0.05$. The wetting time $\tau$ is given by

$$\tau(\vec{x}, t) = \tau_0(\vec{x}) + \int_0^t \chi_{\Omega(s)}(\vec{x})\, ds, \tag{5.5}$$

where $\vec{x} = (x, y)$. We suppose that the left-half plane $x < x_0$, where $x_0 = -0.585$, has been wetted, with initial wetting time

$$\tau_0(\vec{x}) = \begin{cases} -\lambda(x - x_0), & \text{if } x - x_0 < 0, \\ 0, & \text{if } x - x_0 \geq 0, \end{cases} \tag{5.6}$$

where $\lambda = 6.538$. The initial contact line is a circle centered at $(x_0, 0)$. As shown in Fig. 10, the wetted region moves into the right-half plane $x > x_0$, and approaches a fixed, approximately elliptical shape that travels with constant velocity. In Table 3, we compare the numerically computed values of the drop velocity and the diameters of the wetted region with the values computed in Sec. 3.2 by perturbation theory. We compute the asymptotic values from (3.28) and (3.30), neglecting the order $\epsilon^2$ terms, using the numerically computed curvature of the traveling drop, which is $\kappa_0 = 0.79$, with associated radius $a_0 = 0.506$ defined in (3.13). There is excellent quantitative agreement.

In Fig. 11 and Fig. 12[2], we show numerical solutions in which the contact line velocity is given by (5.1), and the static contact angle $\theta_S$ is given by

$$\theta_S = \begin{cases} \tau/T, & \text{if } 0 \leq \tau \leq T, \\ 1, & \text{if } \tau > T. \end{cases} \tag{5.7}$$

[2]In our implementation, we use an adaptive time step. We save the level set function at every certain steps to analyze the results. Therefore the data shown on the figures are the results at recorded time which can be arbitrary non-negative real numbers.

| | $V$ | $d_x$ | $d_y$ |
|---|---|---|---|
| Asymptotic | 0.0356 | 1.055 | 1.211 |
| Numerical | 0.0364 | 1.06 | 1.22 |

Table 3: A comparison of the asymptotic values of the velocity $V$ and the $x$ and $y$ diameters $d_x$ and $d_y$ of the wetted region with values obtained from the numerical solution shown in Fig. 10.

The only difference between Fig. 11 and Fig. 12 is that $\theta = |\nabla h|$ in Fig. 11 and $\theta = \tan^{-1}(|\nabla h|)$ in Fig. 12. The difference is hardly noticeable.

The wetting time $\tau$ is given by (5.5), with an initial wetting time (5.6) where $\lambda = 0.1$ and $x_0 = 0$. The initial contact line is a circle centered at $(0, 0)$. We show solutions for various values of the deposition timescale $T$. In Fig. 11 (a)–(b), where $T = 0.5$, and Fig. 11 (c), where $T = 5.0$, the wetted region moves to the right into the initially unwetted right-half plane, because of the initial wetting time gradient, and distorts because of the effects of surfactant deposition. The wetted region continues moving to the right with an approximately constant velocity. The shape of the wetted region is roughly constant, except for the formation of thin liquid trails at the top and bottom edges in Fig. 11 (b). In Fig. 11 (d), where $T = 50$, the wetted region expands, and we do not see the formation of a traveling drop on the timescale of our numerical solutions. This behavior is in qualitative agreement with the experiments, where a drop of a sufficiently dilute solution of HDT expands and spreads out across the entire surface.

The distortion of the wetted region into a traveling crescent shape seen in Fig. 11 (a)–(c) is qualitatively similar to experimental observations of reactive autophobic spreading. The shape of the traveling drop in Fig. 11 (b) for $T = 0.5$ is strikingly similar to the experimentally observed shape of the drop shown in Fig. 5 (c) of [2]. The liquid trails that form at the edges of the wetted region in the numerical solution are more oblique than the ones observed in the experiment, presumably because the contact lines pin in the experiment. The trails may not be fully resolved in our numerical solutions. They do not appear in the coarser grid solutions, and on intermediate grids we may see the formation of only one of the trails. The trails persist under grid refinement, however, as illustrated in Fig. 15 (a)–(b) below.

In Fig. 13, we show a plot of the drop height at different times for the case $T = 5$, and in Fig. 14, we show a colormap of the wetting time. The wetting time color map indicates the amount of surfactant deposited by the drop, with a wetting time of $\tau \geq 5$ corresponding to a fully organized SAM.

In Fig. 15, we show a set of solutions with different initial data for the wetting time. The contact line velocity is given by (5.1), and the static contact angle is given by (5.7). The initial wetting time is

$$\tau_0(x, y) = \begin{cases} 1 - [(x - x_0 + r_0)^2 + y^2]/\epsilon^2, & \text{if } (x - x_0 + r_0)^2 + y^2 < \epsilon^2, \\ 0, & \text{otherwise.} \end{cases} \tag{5.8}$$

The initial location of the contact line is

$$(x - x_0)^2 + y^2 = r_0^2. \tag{5.9}$$

This initial data corresponds to a partially wetting, circular surface heterogenity, centered at $x_0 - r_0$, located at the left edge of a circular wetted region, centered at $x_0$. In the solutions, the

radius of the heterogeneity is $\epsilon = 0.1$, and the radius of the wetted region is $r_0 = 0.5$. The overall shapes of the wetted regions are similar to those of the wetted regions in Fig. 11.

Finally, we show some numerical solutions that include contact angle hysteresis. The contact line velocity is given by (2.9):

$$V_n = \begin{cases} (\theta - \theta_A)^m & \text{if } \theta \geq \theta_A, \\ 0 & \text{if } \theta_R < \theta < \theta_A, \\ -(\theta_R - \theta)^m & \text{if } \theta \leq \theta_R. \end{cases} \tag{5.10}$$

We observe a variety of different behaviors, depending of the choice of the exponent $m$, and the expressions for $\theta_A$ and $\theta_R$. We will present a few illustrative solutions without attempting to explore all of the possible behaviors. We suppose that the advancing and receding contact angles are given by

$$\theta_A = \begin{cases} \alpha_A \tau/T, & \text{if } 0 \leq \tau \leq T, \\ \alpha_A, & \text{if } \tau > T, \end{cases} \qquad \theta_R = \begin{cases} \alpha_R \tau/T, & \text{if } 0 \leq \tau \leq T, \\ \alpha_R, & \text{if } \tau > T, \end{cases} \tag{5.11}$$

where $\alpha_A = 1.2$, $\alpha_R = 1.0$. The solutions for $m = 1$ appear similar to the previous solutions for $m = 1$ without contact angle hysteresis. The solutions for $m = 3$ evolve more slowly than the ones for $m = 1$, and the wetted regions deform less. This is presumably because $\theta - \theta_A$, or $\theta - \theta_R$, is less than 1 at the contact line, so the cubic power law dependence with $m = 3$ in (5.10) leads to smaller contact line velocities that the linear dependence with $m = 1$.

Finally, we show a grid refinement analysis for the example above in Fig. 18 to see how well our method deal with the less regular flow. The mesh lines are taken as $N = 50, 100, 200$, and 300. All the simulations are qualitatively and quantitatively similar in terms of the position and the size of the droplet. But only reasonably fine grids ($N = 200, 300$ in this case) can capture the fine structure of the tail.

# 6 Conclusions

We have formulated a model for the reactive autophobic spreading of drops, and developed a numerical scheme, based on the level set method and the immersed interface method, to compute numerical solutions of this model. The numerical solutions of traveling drops agree qualitatively with experimental observations, and quantitatively with analytical solutions of the model equations. Further work is required to make quantitative comparisons between experimental measurements and numerical solutions, to use more detailed models of the fluid hydrodynamics and surfactant transport near the contact line, and to extend our numerical scheme to solve these more detailed models.

**Acknowledgments.** N. Abbott showed us his unpublished experiments on the autophobic spreading and pinning of drops, and made numerous helpful remarks on this problem. A. Mogilner provided information on cell motion. The work of J. K. Hunter was partially supported by the NSF under grant number DMS-0072343. The work of Z. Li was partially supported by the NSF under grant number DMS-96-26703, North Carolina State FR&PD Fund, and the ARO under grant number 39676-MA. The work of H. Zhao was partially supported by the NSF under grant number DMS-97-06566.

## References


[1] J. D. Andrade, D. E. Gregonis, and L. M. Smith, in *Surface and Interfacial Aspects of Biomedical Polymers*, Vol. 1, ed. J. D. Andrade, Plenum, New York, 1985.

[2] H. A. Biebuyuck, and G. Whitesides, Autophobic pinning of drops of alkanethiols on gold, *Langmuir* (1994), **10**, 4581–4587.

[3] R. J. Braun, B. T. Murray, W. J. Boettinger, and G. B. McFadden, Lubrication theory for reactive spreading of a thin drop, *Phys. Fluids* (1995), **7**, 1797–1810.

[4] R. A. Drawhor, and N. Abbott, Anchoring of nematic liquid crystals on self-assembled monolayers formed from alkanethiols on semi-transparent films of gold, *J. Phys. Chem.* (1995), **99**, 16511–16515.

[5] L. H. Dubois, and R. G. Nuzzo, Synthesis, structure, and properties of model organic surfaces, *Annu. Rev. Phys. Chem.* (1992), **43**, 437–463.

[6] E. B. Dussan V., On the spreading of liquids on solid surfaces: static and dynamic contact lines, *Ann. Rev. Fluid Mech.* (1979), **11**, 371–400.

[7] P. Ehrhard, and S. H. Davis, Non-isothermal spreading of liquid drops on horizontal plates, *J. Fluid Mech.* (1991), **229**, 365–388.

[8] M. L. Ford, and A. Nadim, Thermocapillary migration of an attached drop on a solid surface, *Phys. Fluids* (1994), **6**, 3183–3185.

[9] N. Eustathopoulos, M. G. Nicholas, and B. Drevet, *Wettability at High Temperatures*, Pergamon Materials Series, Vol. 3, Pergamon, Amsterdam, 1999.

[10] P. G. de Gennes, Wetting: statics and dynamics, *Rev. Modern Phys.* (1985), **57**, 827–863.

[11] D. Gilbarg, and N. S. Trudinger, *Elliptic Partial Differential Equations of Second Order*, Springer-Verlag, New York, 1977.

[12] H. P. Greenspan, On the motion of a small viscous droplet that wets a surface, *J. Fluid Mech.* (1978), **84**, 125–143.

[13] P. J. Haley, and M. Miksis, The effect of the contact line on droplet spreading, *J. Fluid Mech.* (1991), **223**, 57–81.

[14] L. M. Hocking, Rival contact-angle models and the spreading of drops, *J. Fluid Mech.* (1992), **229**, 671–681.

[15] T. Hou, Z. Li, S. Osher, and H. Zhao, A hybrid method for moving interface problems with application to the Hele-Shaw flow, *J. Comput. Phys.* (1997), **134**, 236–252.

[16] J. Lee, A. Ishihara, J.A. Theriot, and K. Jacobson, Principles of locomotion of simple shaped cells, *Nature* (1993), **362**, 161–171.

[17] L. Leger, and J. F. Joanny, Liquid spreading, *Rep. Prog. Phys.* (1992), 431–486.

[18] R. J. LeVeque, and Z. Li, The Immersed Interface Method for Elliptic Equations with Discontinuous Coefficients and Singular Sources, *SIAM J. Numer. Anal.* (1994), **31**, 1019-1044.

[19] Z. Li, The Immersed Interface Method — A Numerical Approach for Partial Differential Equations with Interfaces, *Ph.D. Thesis* (1994), University of Washington.

[20] Z. Li, A Fast Iterative Algorithm for Elliptic Interface Problems, *SIAM J. Numer. Anal.* (1998), **35**, 230–254.

[21] Z. Li, H. Zhao, and H. Gao, A Numerical Study of Electro-migration Voiding by Evolving Level Set Functions on a Fixed Cartesian Grid, *J. Comput. Phys.* (1999), **152**, 281-304.

[22] D. R. Linde, ed., *The CRC Handbook of Chemistry and Physics*, 73rd ed., CRC Press, Boca Raton, 1992.

[23] A. Mogilner, and G. Oster, The physics of lamellipodial protrusion, *European Biophysical Journal* (1996), **25**, 47–53.

[24] A. Oron, S. H. Davis, and S. G. Bankoff, Long-scale evolution of thin liquid films, *Rev. Mod. Phys.* (1997), **69**, 931–980.

[25] S. Osher, and J.A. Sethian, Fronts propagating with curvature-dependent speed: Algorithms based on Hamilton-Jacobi formulations, *J. Comput. Phys.* (1988), **79**, 12-49.

[26] J. A. Sethian, Level Set Methods and Fast Marching methods, *Cambridge University Press* (1999), 2nd edition.

[27] M. K. Smith, Thermocapillary migration of a two-dimensional liquid droplet on a solid surface, *J. Fluid Mech.* (1995), **24**, 209–230.

[28] M. Sussman and P. Smereka and S. Osher, *J. Comput. Phys.* (1994), **114**.

[29] D. Peng, B. Merriman, S. Osher, H.K. Zhao, M. Kang, A PDE Based Fast Local Level Set Method, *J. Comput. Phys.* (1999), **155**, 410-438.

# List of Figures

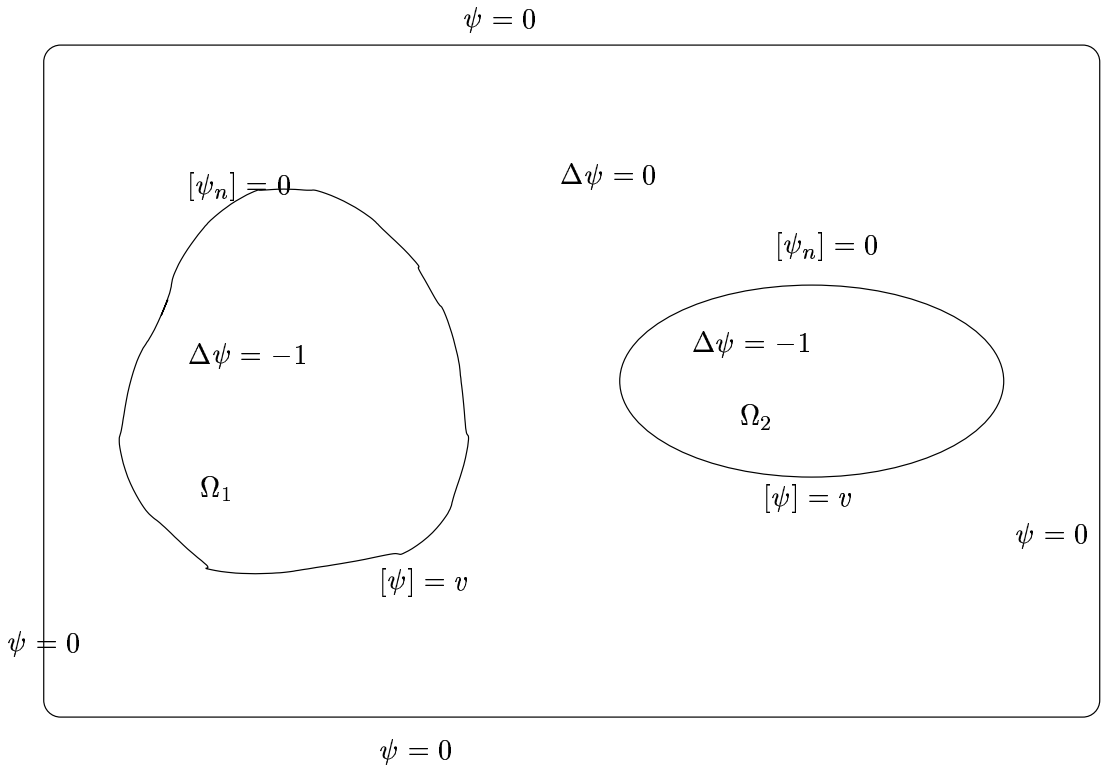


Figure 1: A sketch of the extension from an irregular to a rectangular domain. In this illustration, there are two drops with corresponding wetted regions $\Omega_1$ and $\Omega_2$.

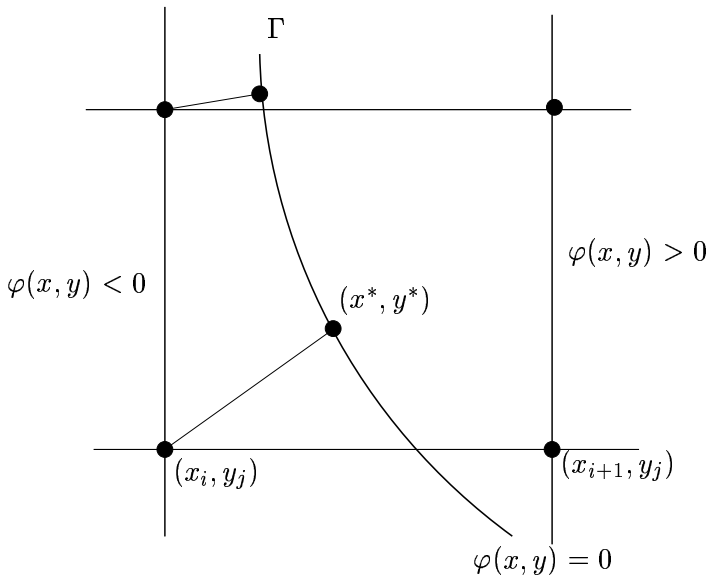


Figure 2: The projection $(x^*, y^*)$ of an irregular grid point $(x_i, y_j)$ on the boundary, where $\varphi(x_i, y_j) < 0$.

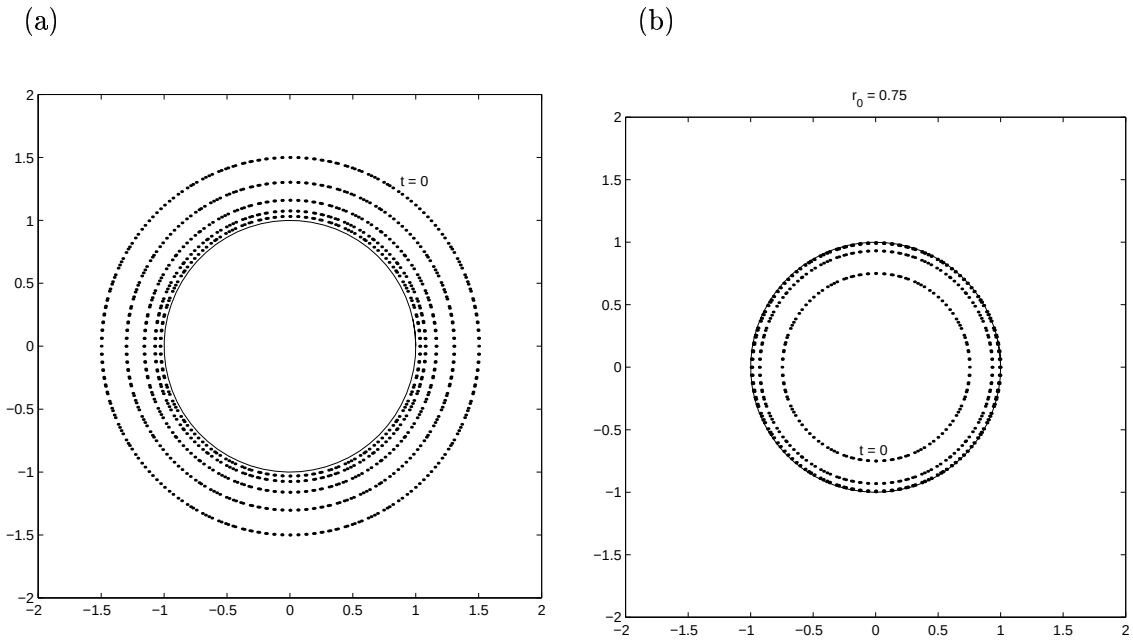


Figure 3: The evolution of a circular contact line on a uniform surface with contact line velocity (5.1), and static contact angle $\theta_S = 0.2$. The drop volume is $q = 0.05\pi$, and the equilibrium radius is $a_0 = 1$. (a) A contracting circle with an initial radius of $r_0 = 1.5$. (b) An expanding circle with an initial radius of $r_0 = 0.75$.

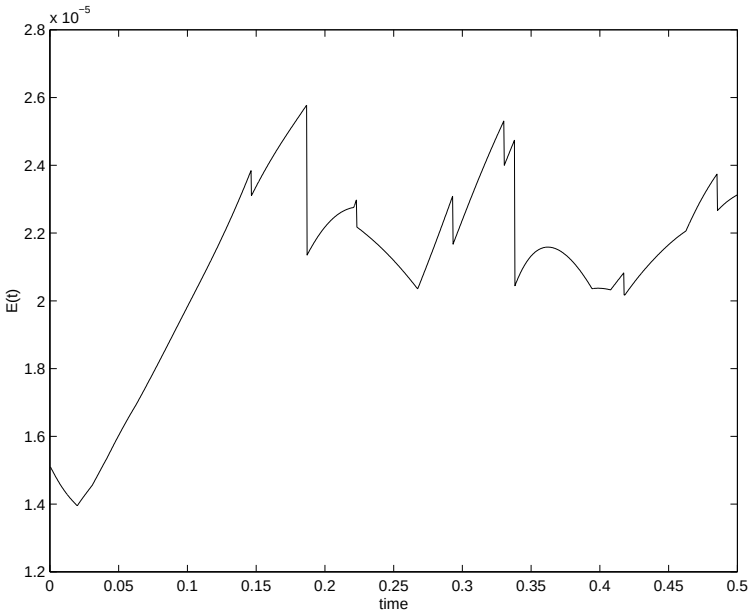


Figure 4: Error plot $E(t)$ defined in (5.2) in time interval $0 \leq t \leq 0.5$. The order of the error is $O(10^{-6})$.

(a)

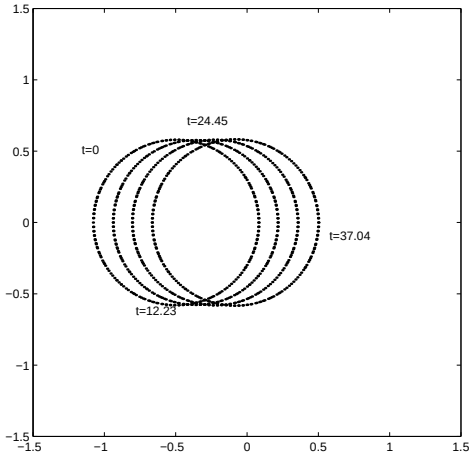


(b)

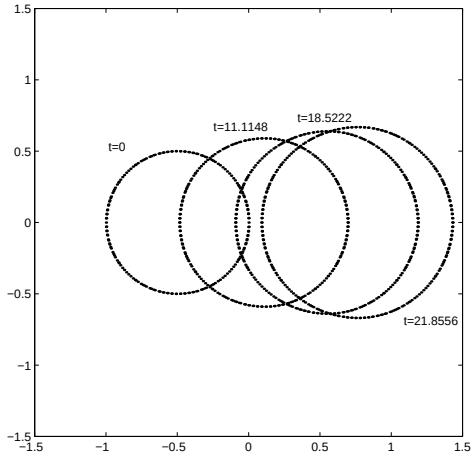


Figure 5: Snap shots of circular wetted regions on a surface with contact line velocity (5.1), and static contact angle $\theta_S = \theta_0(1 - \lambda x)$. The volume is $q = 0.01\pi$, and $\theta_0 = 0.2$. (a) $a_0 = 0.58$ and $\lambda = 0.1$. (b) $a_0 = 0.5$ and $\lambda = 0.5$.

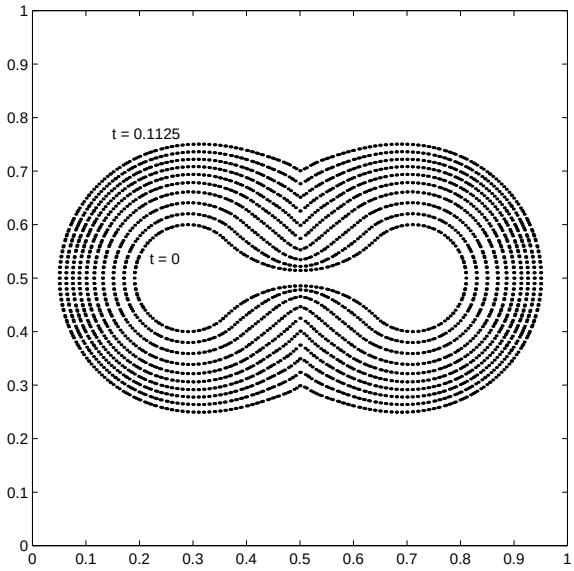


Figure 6: The evolution of a dumbbell shaped wetted region on a surface with contact line velocity (5.1), a uniform static contact angle $\theta_S = 0.2$, and volume $q = (0.05)\pi(0.5)^3$. The region expands outward.

(a)

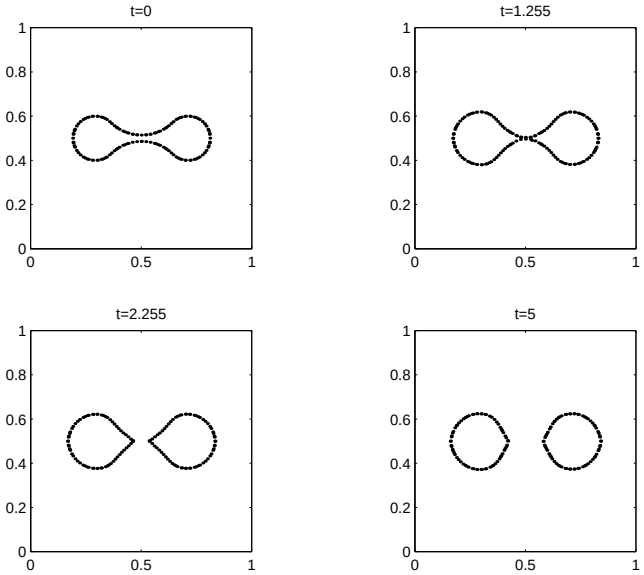


Figure 7: The evolution of a dumbbell shaped wetted region on a surface with contact line velocity (5.1), a uniform static contact angle $\theta_S = 0.2$, and volume $q = (0.05)\pi(0.2)^3$. The region contracts and splits.

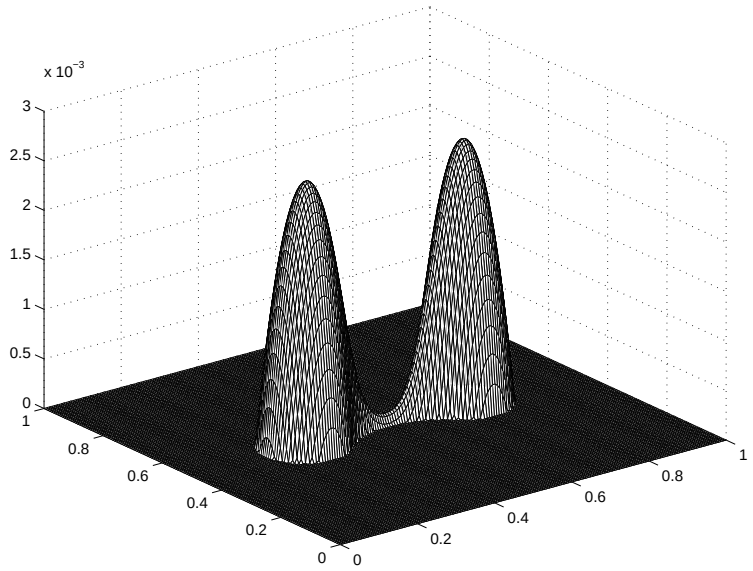


Figure 8: The surface plot of the solution to the normalized Poisson equation $-\Delta\psi = 1$ with $\psi = 0$ at the boundary of the initial dumbbell in Fig. 7.

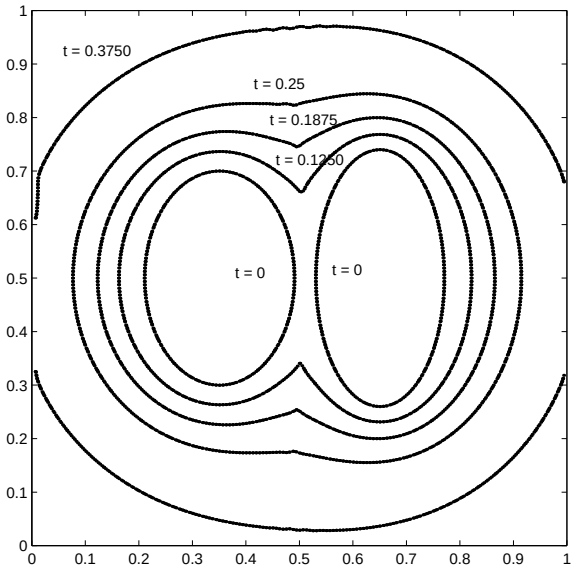


Figure 9: The merging of the two ellipses in (5.3). The surface has contact line velocity (5.1), a uniform static contact angle $\theta_S = 0.2$, and the total volume of the two drops is $q = 0.05\pi$.

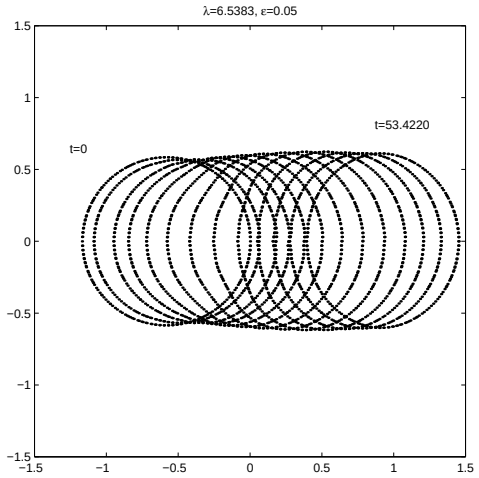


Figure 10: The motion of the contact line on a surface with contact line velocity (5.1), and static contact angle (5.4)–(5.5), with $\theta_0 = 0.2$ and $\epsilon = 0.05$. The volume of the drop is $q = 0.01\pi$. The initial wetting time is given by (5.6) with $\lambda = 6.538$ and $x_0 = -0.585$. The initial location of the contact line is a circle in the left-half plane centered at $(-0.585,\ 0)$ with radius 0.585. The drop approaches an elliptically shaped traveling drop.

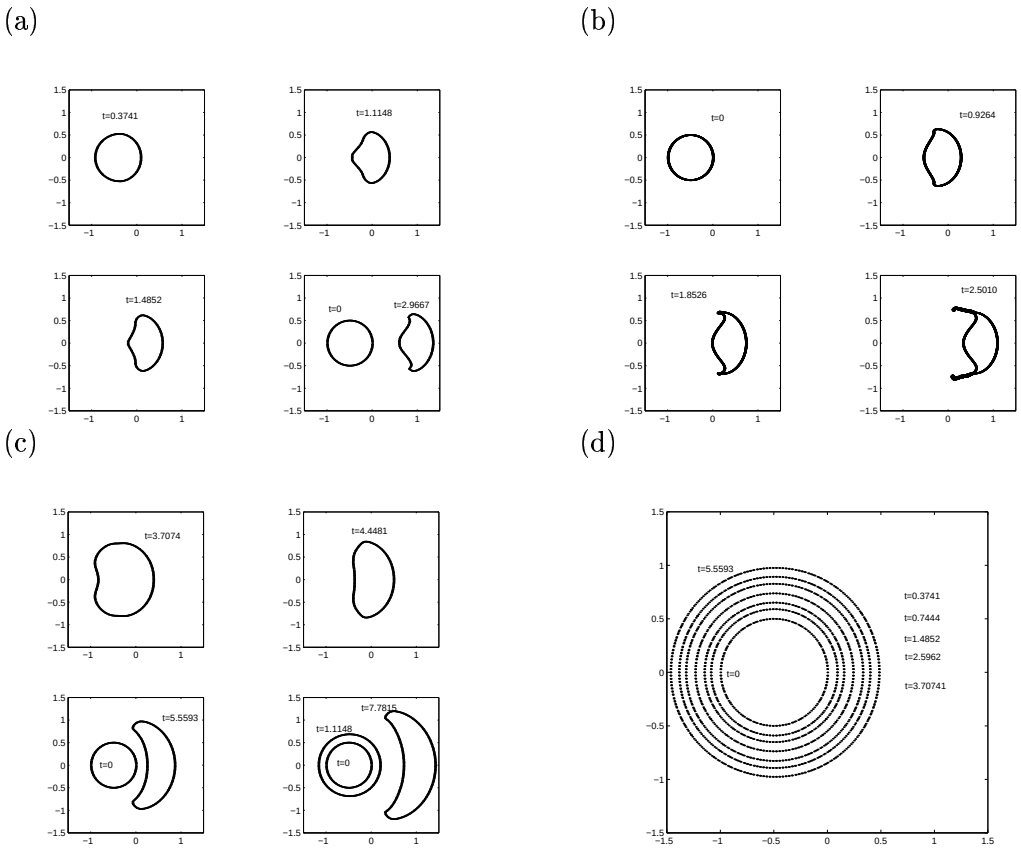


Figure 11: The motion of the contact line on a surface with contact line velocity (5.1). The static contact angle is given by (5.7), the wetting time by (5.5), and the initial wetting time by (5.6), with $\lambda = 0.1$ and $x_0 = 0$. The initial location of the contact line is a circle in the left-half plane centered at $(-0.5,\ 0)$ with radius 0.5, and the volume of the drop is $q = 0.01\pi$. The solutions are shown for various deposition timescales: (a)–(b) $T = 0.5$; (c) $T = 5$; (d) $T = 50$. The solutions in (a), (c), (d) were computed on a $100 \times 100$ grid, and the solution in (b) was computed on a $400 \times 400$ grid. The contact lines move from left to right in (a)–(c), and expand in (d). The times at which the contact lines are plotted are shown in the figures.

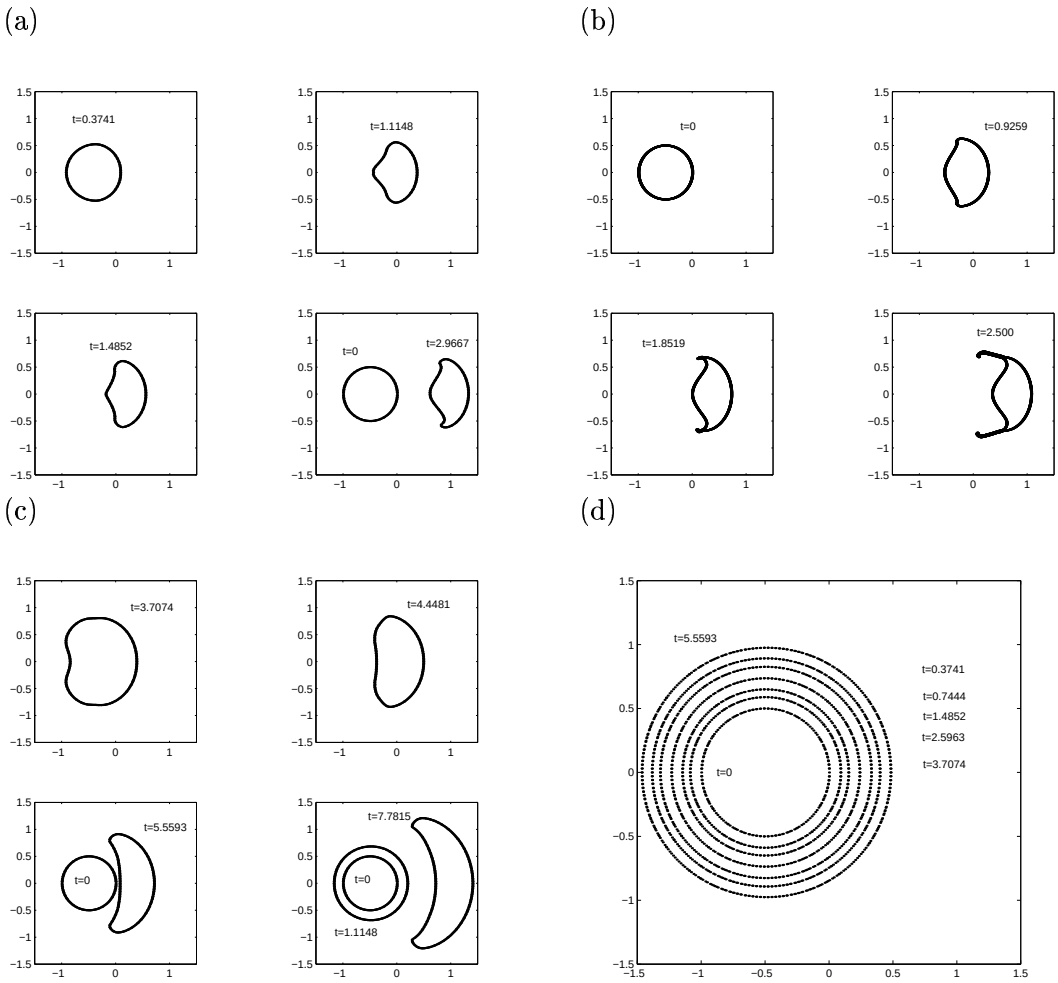


Figure 12: The motion of the contact line on a surface with contact line velocity (5.1). The parameters are exact the same as in Fig. 11 except now the dynamic contact angle of the drop is given by $\tan\theta = |\nabla h|$. We can see that the motion of the contact line is similar to that in Fig. 11. The only noticeable difference is in the position of the contact line in (c).

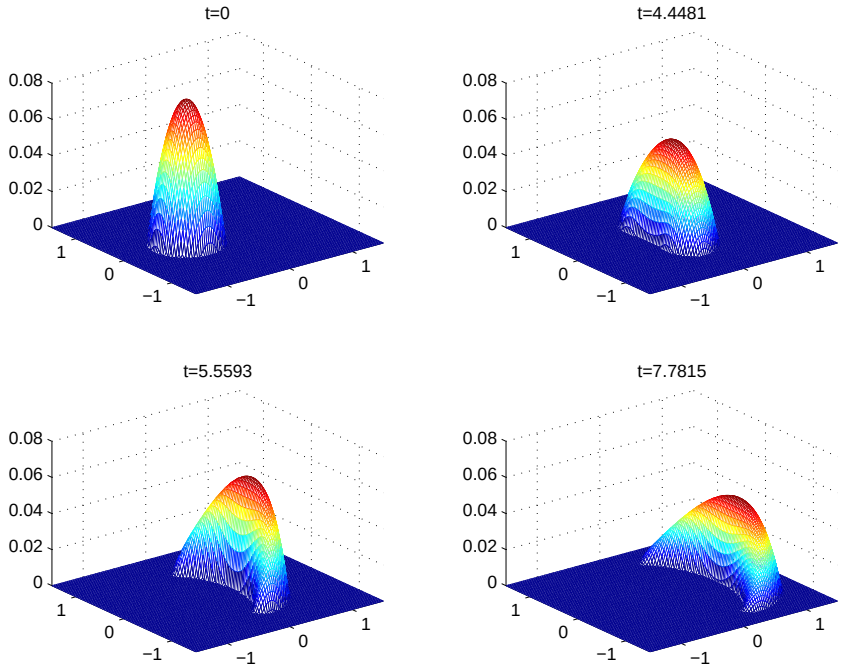


Figure 13: The height $h$ of the drop at different times for the solution in Fig. 11 (c).

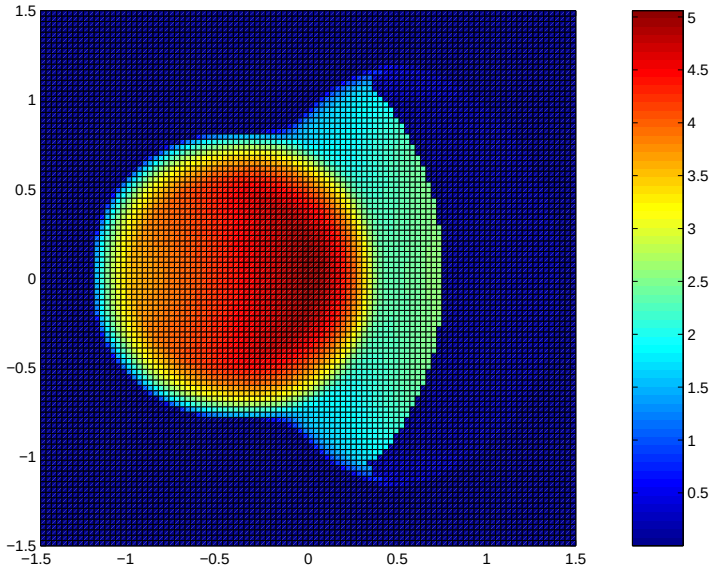


Figure 14: A colormap of the wetting time $\tau$ for the solution in Fig. 11 (c).

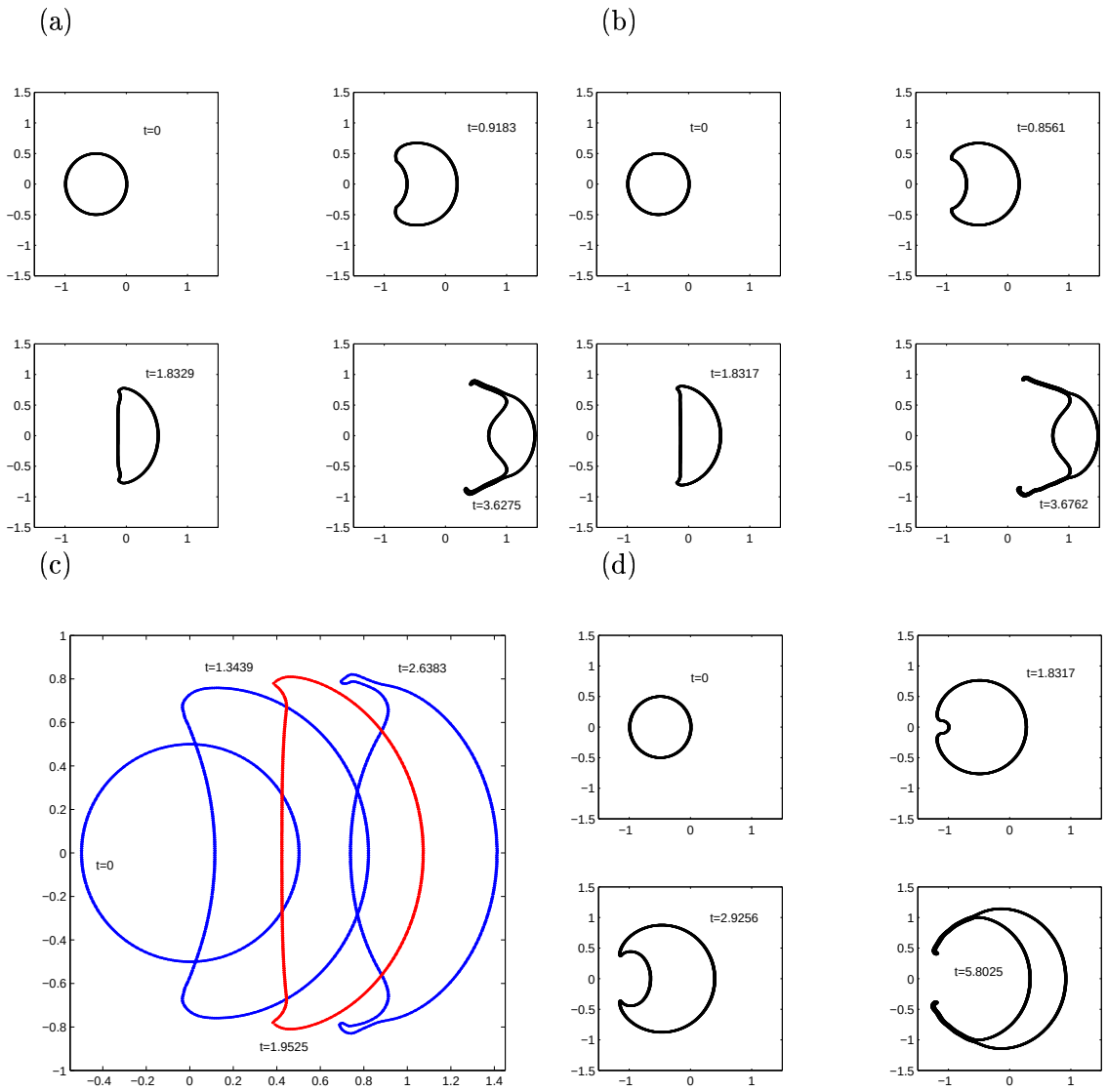


Figure 15: The motion of the contact line on a surface with contact line velocity (5.1) and (5.7). In (a)–(c), we use $T = 0.5$ and $q = 0.1/\pi$. In (d), we use $T = 5.0$, and $q = 0.1/\pi$. In (a), (b), (d) the initial location of the contact line is a circle (5.9) of radius $r_0 = 0.5$ centered at $(x_0, 0)$ with $x_0 = -0.5$. The initial wetting time is given by (5.8) with $\epsilon = 0.1$. In (c), we use the same data as in (a), except that $x_0 = 0$. The solution shown in (a) is computed on a $200 \times 200$ grid, and the solutions shown in (b)–(d) are computed on a $300 \times 300$ grid.

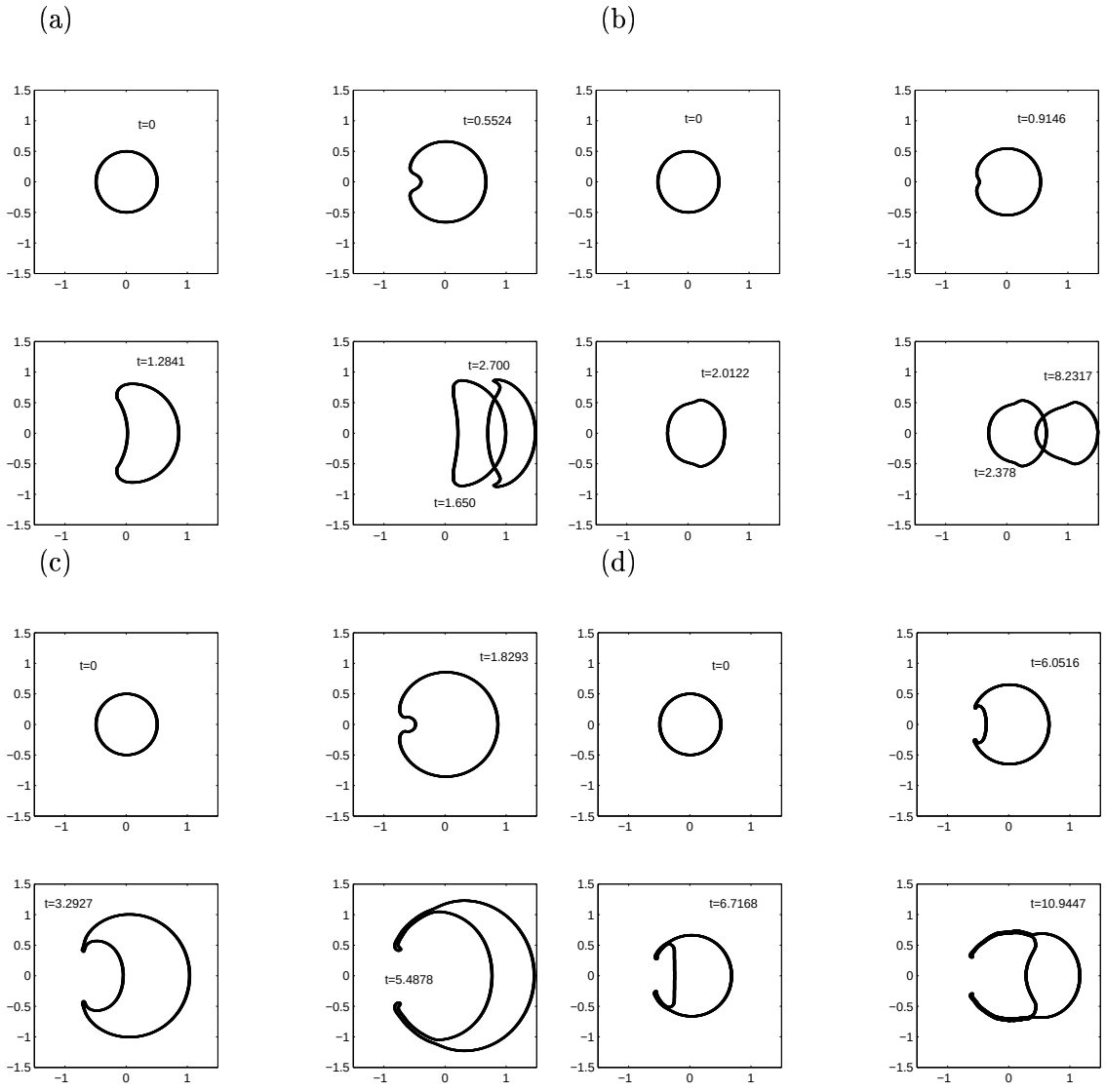


Figure 16: Numerical solutions with contact angle hysteresis. The contact line velocity is given by (5.10), and the advancing and receding contact angles are given by (5.11) with $\alpha_A = 1.2$, $\alpha_R = 1$. The drop volume is $q = 0.0157\pi$. The solutions are computed on a $200 \times 200$ grid except in (d) which is computed on a $300 \times 300$ grid. (a) $T = 0.5$, $m = 1$; (b) $T = 0.5$, $m = 3$; (c) $T = 5$, $m = 1$; (d) $T = 5$, $m = 3$.

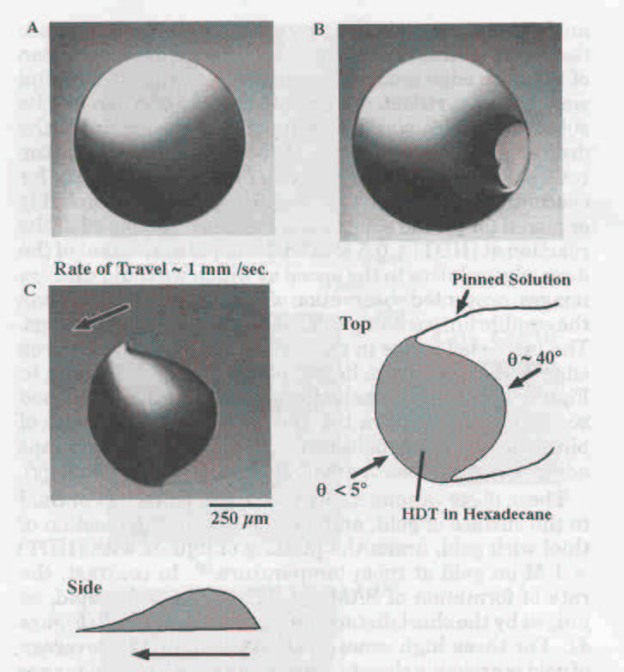


Figure 17: An experiment result from [2]. The caption from [2] reads: *Drops of 1 mM HDT in hexadecane moved, and were not pinned, across the surface of bare gold at rates of* $\sim 1mm/s$. *The volume of these drops was* $\sim \mu L$. *(A) The drop shape after* 1.267 *s of contact with the bare gold surface. (B) The drop* 0.067 *s later than A, begins to dewet the gold because SAM formation results in a finite contact angle between the drop and the surface. (C) The drop* $2,000$ *s later than B, pushed forward at a steady rate of* 1 *mm/s.* The results agree with the simulations in Fig. 16, Fig. 18, and some of simulations in Fig. 15 qualitatively.

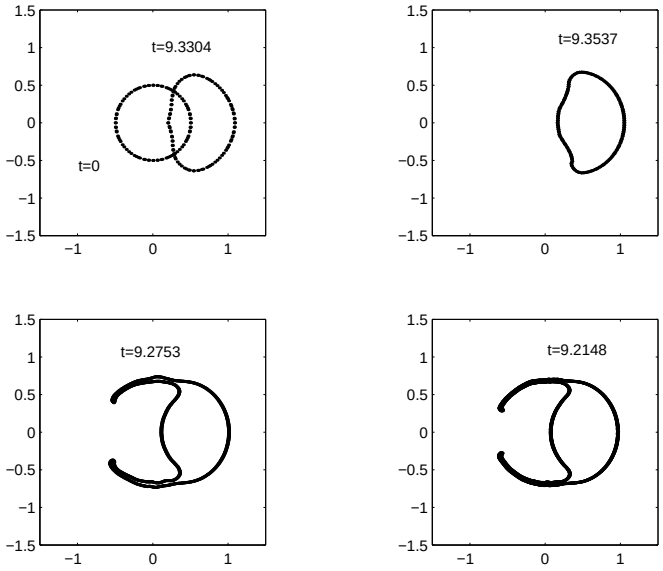


Figure 18: A grid refinement analysis with $50 \times 50$, $100 \times 100$, $200 \times 200$, and $300 \times 300$ grids. The contact line velocity is given by (5.10), and the advancing and receding contact angles are given by (5.11) with $\alpha_A = 1.2$, $\alpha_R = 1$, $T = 5$, $m = 3$. The drop volume is $q = 0.0157\pi$. We use the relation $\tan\theta = |\nabla h|$. We see similar qualitative and quantitative behavior, but the find grid gives better resolution for the tails.